



RESEARCH ARTICLE

10.1029/2022MS003210

Special Section:

Advances in scaling and modeling of land-atmosphere interactions

Key Points:

- We implemented a 1D multilayer canopy scheme at every gridpoint in the Dutch Atmospheric Large Eddy Simulation resolving leaf, canopy and boundary layer scales as a continuum
- The model is compared against a data set gathered during the Amazonian dry season, showing that wind and temperature are better represented than humidity
- We present the first Large Eddy Simulations validation of in-canopy CO₂ processes

Correspondence to:

X. Pedruzo-Bagazgoitia,
xabier.pedruzo@ecmwf.int

Citation:

Pedruzo-Bagazgoitia, X., Patton, E. G., Moene, A. F., Ouwersloot, H. G., Gerken, T., Machado, L. A. T., et al. (2023). Investigating the diurnal radiative, turbulent, and biophysical processes in the Amazonian canopy-atmosphere interface by combining LES simulations and observations. *Journal of Advances in Modeling Earth Systems*, 15, e2022MS003210. <https://doi.org/10.1029/2022MS003210>

Received 26 MAY 2022

Accepted 23 DEC 2022

© 2023 The Authors. Journal of Advances in Modeling Earth Systems published by Wiley Periodicals LLC on behalf of American Geophysical Union. This is an open access article under the terms of the Creative Commons Attribution License, which permits use, distribution and reproduction in any medium, provided the original work is properly cited.

Investigating the Diurnal Radiative, Turbulent, and Biophysical Processes in the Amazonian Canopy-Atmosphere Interface by Combining LES Simulations and Observations

X. Pedruzo-Bagazgoitia^{1,2} , E. G. Patton³ , A. F. Moene², H. G. Ouwersloot² , T. Gerken⁴ , L. A. T. Machado^{5,6}, S. T. Martin⁷ , M. Sörgel⁸ , P. C. Stoy⁹ , M. A. Yamasoe¹⁰ , and J. Vilà-Guerau de Arellano^{2,8} 

¹ECMWF, Bonn, Germany, ²Meteorology and Air Quality Section, Wageningen University Research, Wageningen, The Netherlands, ³National Center for Atmospheric Research, Boulder, CO, USA, ⁴School of Integrated Sciences, James Madison University, Harrisonburg, VA, USA, ⁵Multiphase Chemistry Department, Max Planck Institute for Chemistry, Mainz, Germany, ⁶Instituto de Física, Universidade de São Paulo, São Paulo, Brazil, ⁷School of Engineering and Applied Sciences, Harvard University, Cambridge, MA, USA, ⁸Atmospheric Chemistry Department, Max Plank Institute for Chemistry, Mainz, Germany, ⁹Department of Biological Systems Engineering, University of Wisconsin-Madison, Madison, WI, USA, ¹⁰Departamento de Ciências Atmosféricas, Instituto de Astronomia, Geofísica e Ciências Atmosféricas, Universidade de São Paulo, Cidade Universitária, São Paulo, Brazil

Abstract We investigate the atmospheric diurnal variability inside and above the Amazonian rainforest for a representative day during the dry season. To this end, we combine high-resolution large-eddy simulations that are constrained and evaluated against a comprehensive observation set, including CO₂ concentrations, gathered during GoAmazon2014/15. We design systematic numerical experiments to quantify whether a multilayer approach in solving the explicit canopy improves our canopy-atmosphere representation. We particularly focus on the relationship between photosynthesis and plant transpiration, and their distribution at leaf and canopy scales. We found the variability of photosynthesis drivers like vapor pressure deficit and leaf temperature to be about 3 times larger for sunlit leaves compared to shaded leaves. This leads to a large spread on leaf stomatal conductance values with minimum and maximum values varying more than 100%. Regarding the turbulent structure, we find wind-driven stripe-like shapes at the canopy top and structures resembling convective cells at the canopy. Wind-related variables provide the best spatiotemporal agreement between model and observations. The potential temperature and heat flux profiles agree with an observed decoupling near the canopy top interface, although with less variability and cold biases of up to 3 K. The increasing complexity on the biophysical processes leads to the largest disagreements for evaporation, CO₂ plant assimilation and soil efflux. The model is able to capture the correct dependences and trends with the magnitudes still differing. We finally discuss the need to revise leaf and soil models and to complete the observations at leaf and canopy levels.

Plain Language Summary Most atmospheric models currently represent the vegetated canopy as one slab layer at the lowest level of the model. This oversimplification leads to limitations in our understanding on how the canopy and the atmosphere interact, as well as when comparing and interpreting model output with real world observations largely influenced by the presence of a canopy. In this study we implemented a more realistic multilayer canopy scheme in a turbulence-resolving atmospheric model. We focused and analyzed the features and changes that appear in atmospheric variables due to the presence of a three-dimensional canopy. To do so we designed several numerical experiments to understand how to best represent the relevant physical and biological processes. We quantified the variability of light, humidity and temperature at leaf-level, and discussed the large variability the features appearing in the lowest atmosphere by the presence of the canopy. We also compare our model simulations with a complete set of atmospheric observations taken inside and above the Amazonian rainforest, and find an overall good agreement. We finally propose future ways to improve the canopy scheme and, in general, simulations including a vegetated canopy.

1. Introduction

The vegetation is a key component of the biophysical processes taking place on and near the Earth's surface. In particular, it plays a critical role on the properties and diurnal evolution of the atmospheric boundary layer (ABL) (Gentine et al., 2019; Helbig et al., 2021). Plant structure alters the flow within the canopy and up to few

hundred meters above the ground within the so called roughness sub-layer (Finnigan et al., 2009). Due to the strong relationship between photosynthesis and plant transpiration, modifications of the flow and radiation within the vegetated canopy are not only important for carbon fluxes, but also for the partitioning of the fluxes of energy and moisture (Cescatti & Niinemets, 2004; Durand et al., 2021). In fact, vegetation is fundamental in coupling the large-scale water and carbon cycles at the very small scales, as both water vapor and CO_2 are exchanged simultaneously through the stomata present in the leaves (Katul et al., 2012). As such, this coupled system can be studied in an integrated manner and connecting processes that take place at leaf, canopy and ABL scales (Vilà-Guerau de Arellano, Ney, et al., 2020).

Despite active vegetation having such a major role on determining the near surface atmospheric conditions, atmospheric models have traditionally used relatively simple vegetation models with a so called big-leaf or, at best, two big-leaf approach (Dai et al., 2004). The big-leaf concept consists on the approximation of a vegetated canopy as a single layer of vegetation responding to the environmental forcings at the lowest model level. The best known example of a one-leaf model is likely the Penman-Monteith equation proposed to calculate canopy evapotranspiration by Monteith (1965). The two-big-leaf approach builds on this approximation by considering shaded and sunlit leaves in that single layer (Dai et al., 2004). Interestingly, the necessary upscaling from leaf to canopy level when using such models is still a current topic of research. While such bulk approach has proved useful to provide some degree of coupling between the surface and the atmosphere, it does not reflect the in-canopy vertical distribution of turbulence and transport of momentum, heat, moisture and other scalars and may provide the correct exchange for incorrect reasons. The simplified vertical distribution of sources and sinks may hinder a correct representation of the magnitude, frequency and spatial features of the exchange between the canopy and the atmosphere above. This mismatch between modeling and reality hampers a correct evaluation when comparing atmospheric models to point observations. An in-depth comparison between the big-leaf and multilayer canopy concepts and their potential and limitations is given by Bonan et al. (2021). As they stressed, the new generation of land surface models will require an explicit approach to solve the thermodynamics of the canopy coupled to ecophysiology and soil processes.

The presence of vegetation alters essentially the vertical distribution of radiation, wind, turbulence and scalars. Therefore, these processes need to be taken into account when simulating explicitly an interactive canopy. Previous research has studied them thoroughly through numerical experiments. Here, we will focus only on canopy-scale turbulence resolving models, for example, Large Eddy Simulations (LES), given the critical role played by turbulence in canopy dynamics. The dynamic effects exerted by the canopy on the near-surface flow have been investigated by Shaw and Schumann (1992), Patton et al. (2003), Finnigan et al. (2009), Maurer et al. (2015), and Ouwersloot et al. (2016), among others. Shaw and Schumann (1992) proposed and implemented in LES the first representation of the drag exerted by a canopy on the near-surface turbulent flow. By using the same concept of canopy momentum drag, Dwyer et al. (1997) presented the first turbulent kinetic energy (TKE) budget based on resolved scales by LES. Patton et al. (2003) further investigated that representation of the canopy and reported that canopies produce turbulence at canopy-scales altering the traditional understanding that turbulent structures continue to diminish in scale with approach toward the ground. Finnigan et al. (2009) further analyzed the canopy-atmosphere interface through LES and described the structures that lead to the sweeps and ejections of air between the canopy and the air above. Ouwersloot et al. (2016) implemented the canopy-drag effects in the Dutch Atmospheric Large Eddy Simulation (DALES) and validated it against previous LES studies as well as wind-tunnel data for a neutrally stable case. For further details, the reader is referred to Brunet (2020), which gives an exhaustive review of the current and historical developments in understanding the turbulent flow within and above the canopy.

Similarly, the modeling of radiation within the canopy has been studied for decades. Most of these attempts have assumed horizontal homogeneity of the canopy and approached the radiative penetration as a one-dimensional problem, with de Wit (1965) and Norman (1979) as the early founders of the later refined in-canopy radiation schemes. In order to somehow account for horizontal spatial heterogeneities, one-dimensional radiative schemes frequently include a leaf-clumping parameter that alters the radiation penetration rate (Fang, 2021; Nilson, 1971). More recently, a computationally much more intensive approach has been suggested where the three-dimensional properties of radiation and canopies are treated (Kobayashi et al., 2012). Using this approach, however, it is currently not computationally feasible to encompass scales that range from leaf to the boundary layer scales and to integrate other relevant processes such as turbulence. Despite the just mentioned numerous examples, not so many studies have attempted to incorporate all mentioned processes into a comprehensive representation of the

canopy and its couplings with the atmosphere. In this sense, the pioneering work by Patton et al. (2016) showed the impact that a fully coupled canopy exerts on a range of stability-varying boundary layer regimes. Due to the full coupling it was possible for them to investigate the impact that a canopy has on near-surface dynamics as well as heat and water vapor fields. One of their main findings was that the canopy-atmosphere exchange is partly regulated by the entire ABL dynamics. However, this study was mostly based on conceptual simulations and only showed a brief validation of the multilayer canopy model by comparing it against the full canopy temperature tendency as observed in the CHATS campaign (Patton et al., 2011). Furthermore, they simplified the impact of CO₂ in the canopy by imposing an homogeneous constant atmospheric CO₂ concentration. Ma and Liu (2019) implemented an integrative canopy scheme in WRF-LES (Powers et al., 2017) solving the canopy energy balance at each vertical level, including the biological effects on varying atmospheric CO₂, and validated in-canopy momentum, heat and moisture fluxes against the mentioned CHATS campaign. They further explored the scalar transport and dynamic impact of a forest edge.

Our broad motivation to focus on the Amazonian rainforest relies on the still open questions that influence key elements of the Earth system. In short, it is not yet well understood the governing processes related to precipitation (Machado et al., 2014) and their interaction with the land (Gentine et al., 2019). Regarding the carbon cycle, it is still an open question whether the Amazonia is shifting from being a carbon sink to a source (Boulton et al., 2022), and the response of the rainforest to droughts (van der Laan-Luijkx et al., 2015). Finally, there is currently a debate on the relationships between surface processes, boundary-layer and clouds in the formation and fate of aerosol particles (Andreae et al., 2018). Our approach toward these challenges, including the coupling of biochemical and physical processes, is here of bottom-up: relating leaf to canopy to boundary-layer scales. The process description is oriented with the goal to advance our understanding on how the small and short spatiotemporal scales occurring at the Amazonian rainforest influence the regional scales.

In the present study we implemented, tested and validated with available observations at the Amazonian rainforest a multilevel canopy model into the Dutch Atmospheric Large Eddy Simulation DALES (Heus et al., 2010; Ouwersloot et al., 2016). By simulating most of the turbulence explicitly, the in-canopy radiative processes, and the leaf energy balance at each vertical level for sunlit and shaded leaves separately we attempt to represent at the essential spatio-temporal scales on orders of meters and seconds the main effects a vegetated canopy exerts on the physics of the ABL. Our aim in this study is to show, first, the possibilities that such a canopy model uncovers. Simulating the leaf scale processes coupled to radiation and explicit ABL dynamics allows us to reveal the high environmental variability at the leaf scale in terms of radiation, vapor pressure deficit (VPD) or leaf temperature (T_{leaf}). Furthermore, we analyze to what extent a bulk or a coarser representation of the canopy hampers the correct representation of within and above canopy dynamics, and test different radiation schemes acting as a forcing at the canopy top. Our second aim is to reveal the main features that appear in the near-surface atmospheric flow in terms of radiation, turbulence, thermodynamics and CO₂, and to what extent it matches real world observations. To that end we simulate a representative case of observed cloudless days in the Amazonian rainforest. The GoAmazon2014/5 project (Fuentes et al., 2016; Martin et al., 2016) deployed a complete set of instrumentation for an extensive characterization of the canopy and the air above. The gathered data includes measurements of radiation and vertical profiles of state variables and turbulent fluxes of typical meteorological variables as well as CO₂-related ones.

2. Methods and Experiment Setup

2.1. Case Description

The analysis in the present study is based on the daily evolution of atmospheric and canopy conditions in the Amazon. The case is based on observations belonging to the GoAmazon 2014/5 project. In particular, this case study aims to be representative for sunny and atmospherically unstable recurrent conditions associated with clear to shallow-cumulus transitions. Those frequent conditions relate, both within and above the canopy, to those happening in the Amazon for the month of September, by the end of the dry season. For that purpose, observations gathered along September 2014 are used to create a representative “aggregate day.” Further details on the case design can be found in Vilà-Guerau de Arellano, Wang, et al. (2020). In this research we focus on the morning transition under clear conditions, a key process in the development of Amazonian boundary-layers.

The simulations start at 8 local time (LT) and end at 16 LT so that they contain the most relevant features of the diurnal variability. A gridbox size of $3 \times 3 \times 3 \text{ m}^3$ and a domain of $3,024 \times 3,024 \times 2,802 \text{ m}^3$ is used in

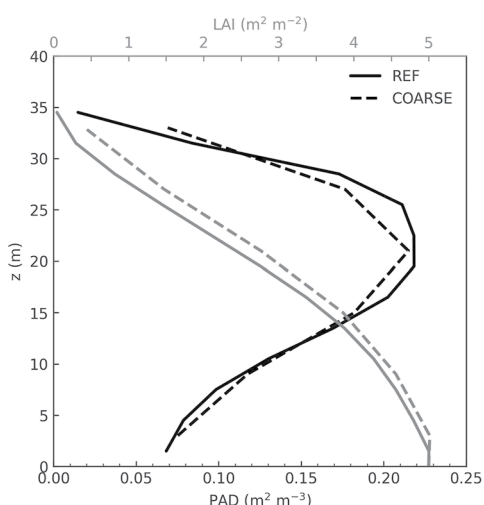


Figure 1. Vertical profiles of prescribed canopy plant area density (PAD) in black and leaf area index (LAI) in gray for REF (full) and COARSE (dashed).

Wang, et al. (2020). The initial atmospheric fields within and near the canopy originally set in Vilà-Guerau de Arellano, Wang, et al. (2020) have been modified to take into account the particular conditions inside and above the canopy. The modifications involved the adjustment of the prescribed initial profiles and canopy settings to better fit inside-and-near canopy observations, and can be found in Appendix A. Note however that the constant and vertically uniform $U = -7 \text{ m s}^{-1}$ and $V = -1 \text{ m s}^{-1}$ winds originally prescribed by Vilà-Guerau de Arellano, Wang, et al. (2020) remain unchanged.

Four numerical experiments were performed in total and are summarized in Table 1. The reference experiment REF uses the mentioned $3 \times 3 \times 3 \text{ m}^3$ gridbox size, a canopy with $\text{LAI} = 5 \text{ m}^2 \text{ m}^{-2}$ spanning across 12 vertical levels and the Delta-Eddington radiation scheme (Joseph et al., 1976; Shettle & Weinman, 1970) for SW and successfully used in previous DALES studies (Barbaro et al., 2013; Pedruzo-Bagazgoitia et al., 2017; Sikma et al., 2019). Since we are interested in studying the in-and-above canopy dynamics under clear-sky conditions, we deactivated cloud formation in DALES for all experiments to avoid additional variability in radiation at canopy top. We also neglect aerosol radiative effects within the simulated domain, and LW is only calculated within the canopy given the relatively small diurnal variability above canopy top. The second experiment RAD is identical to REF except in the SW computation, where the more accurate but computationally expensive RRTMG scheme is used (Iacono et al., 2008). The purpose of RAD is to show that a faster and simpler radiation scheme, that is, the Delta-Eddington scheme, is able to properly simulate the diurnal solar cycle at the canopy top. The main difference between Delta-Eddington and RRTMG in what concerns our study is that the former uses an approximation for the reflection and transmission of light. Furthermore, the Delta-Eddington employed considers only liquid water to interact with radiation, in contrast with RRTMG where the shortwave radiation scattering by methane, water vapor, CO_2 and other chemical species is calculated. At this latitude and time of the year the sun rises and sets at around 6 and 18 LT respectively. Regardless the radiation scheme used, all simulations reproduce the diurnal cycle of SW radiative forcing near the surface. The third numerical experiment COARSE

explores whether a coarser resolution is sufficient to reproduce with similar accuracy the state of the canopy and the interactions between the canopy and the atmosphere above. To that end COARSE employs the same domain but with a $6 \times 6 \times 6 \text{ m}^3$ gridbox size resulting in almost 9 times fewer gridpoints than REF. The difference between the last numerical experiment BULK and REF is that the former uses the zero-order or bulk canopy model previously available in DALES (Pedruzo-Bagazgoitia et al., 2017; Ronda et al., 2001; Vilà-Guerau de Arellano et al., 2014) and similar to what other LES and meteorological models employ. Such comparison allows to quantify the effects typically missed by most models when the canopy vertical heterogeneity, turbulent flow and vegetation response is fully parameterized and

Table 1
Overview of the Performed Numerical Experiments With Their Most Relevant Settings

Name	SW radiation scheme	Canopy model	Gridbox size (m^3)
REF	Delta-Eddington	Multi-layer	$3 \times 3 \times 3$
RAD	RRTMG	Multi-layer	$3 \times 3 \times 3$
COARSE	Delta-Eddington	Multi-layer	$6 \times 6 \times 6$
BULK	Delta-Eddington	Bulk	$3 \times 3 \times 3$

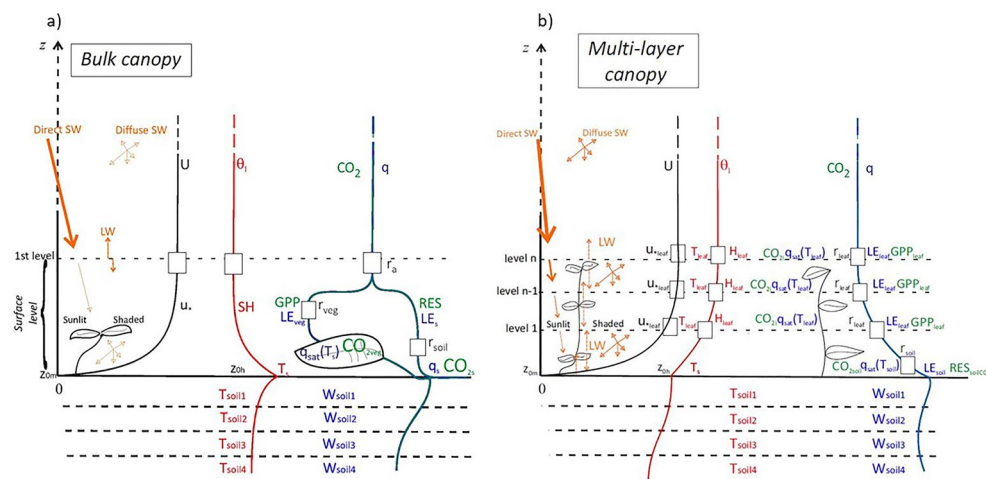


Figure 2. Schematic illustration of the processes and variables involved in the traditional 0-order or bulk canopy scheme used in most atmospheric models (left) and the implemented multilayer canopy in the present study (right).

limited to take place at the surface level (see Figure 2). We assumed in BULK a displacement height $d = 30$ m equal to the height of the lowest tree tops in the canopy for a fair comparison with the other experiments.

The following sections deal with the specifics of the LES model and the multilayer canopy implementation, and the observations used to constrain and validate the numerical experiments.

2.2. The DALES Model and Canopy-Model Implementation

The Dutch Atmospheric Large Eddy Simulation is a LES model under constant development since the 1970s (Cuijpers & Duynkerke, 1993; Heus et al., 2010; Nieuwstadt & Brost, 1986). The starting point for this study is DALES 4.2, where the multilayer canopy model and leaf energy balance have been implemented. Concerning the model parts of interest for this study, three pieces of work paved the way for the multilayer interactive canopy scheme presented here. The mechanistic A-gs model, based on plant physiological aspects at leaf level, was developed by Jacobs and de Bruin (1997) and upscaled to represent the entire canopy by Ronda et al. (2001). This A-gs scheme has been used successfully for almost 10 years in DALES to predict surface fluxes, including the CO₂ flux, based on the response of plant stomata to soil, radiative and atmospheric conditions (Vilà-Guerau de Arellano et al., 2014). Recently, van Diepen et al. (2022) found similar responses of net photosynthesis to PAR and CO₂ in A-gs compared to the well-known Farquhar model (Farquhar et al., 1980). Ouwersloot et al. (2016) implemented in DALES the drag and dynamic effects of rough elements in a neutral turbulent flow and compared it with laboratory experiments. They demonstrated that DALES could correctly reproduce the dynamic effects on the flow of an inert canopy at the lowest vertical levels, both within and above the canopy. Meanwhile, an initial shortwave radiative transfer scheme for the sub-grid canopy was proposed and tested for DALES (Pedruzo-Bagazgoitia et al., 2017). This 2 big-leaf scheme permitted the vegetated surface to react differently to diffuse and direct radiation given their distinct penetration rates along the canopy. With the implementation showed here, the work toward a fully interactive multilayer canopy in DALES moves one step forward.

In short, the single-column canopy model is implemented at every canopy gridbox and is based on that by Patton et al. (2016). Its functioning can be described in 4 steps. First, both the upwards and downwards components of bulk shortwave (SW) and longwave (LW) radiation profiles are calculated at each gridpoint using a single-column radiation scheme. The original shortwave radiation scheme is described in Pedruzo-Bagazgoitia et al. (2017) and has been modified based on the work by Goudriaan and van Laar (1994) for an improved conservation of energy and representation of radiation absorbed by the ground. The scheme represents the vegetation as a homogeneous sub-grid mesh and, given the downward SW at the canopy top, calculates the vertical profiles of downward direct and diffuse components as well as upward shortwave radiation. In addition, it also provides the absorbed SW radiation by sunlit and shaded leaves at each vertical level, the effective canopy albedo for direct and diffuse SW and the radiation absorbed by the ground vegetation and the soil. Clumping of leaves is considered, as it is

frequently done (Williams et al., 2017), by introducing a modulating factor between 0 and 1 that modifies the exponential shape of the radiation extinction coefficient. We show a brief validation of the scheme for Amazonian conditions in Appendix B. As for the in-canopy LW, the scheme follows Patton et al. (2016) and assumes LW received by leaves to be dependent solely on the local air temperature for shaded leaves and on both the local air as well as apparent clear-sky emissivity (Brutsaert, 1975) for sunlit leaves. Being a single-column model, it neglects horizontal radiation fluxes across neighboring columns.

The second step consists on the computation of the leaf energy balance for sunlit and shaded leaves at each vertical level through an iterative method. In earlier work, DALES relied on an A-gs model to determine the canopy's bulk stomatal conductance using a two big-leaf approach (Pedruzo-Bagazgoitia et al., 2017). Here, we closely follow Patton et al. (2016) by extending DALES' plant physiological-mechanistic A-gs model vertically through the canopy to obtain vertically resolved leaf-level temperature, stomatal conductance and heat, moisture fluxes based on the radiative and environmental local conditions for sunlit and shaded leaves separately. It is important to note that the vertical integration of leaf-level stomatal conductance does not necessarily equal the bulk canopy stomatal conductance due to non-linearities in the Penman-Monteith equation, see Bonan et al. (2021). Consistent with Patton et al. (2016), we follow Nikolov et al. (1995) to solve the leaf energy balance, and rely on both Leuning et al. (1995) and Nikolov et al. (1995) when calculating leaf boundary layer conductance. Different from Patton et al. (2016) where leaf-level stomatal conductance responded to a constant atmospheric CO₂ concentration, we transport CO₂ in DALES and hence photosynthesis controls on stomatal conductance are now influenced by time- and space-evolving atmospheric CO₂ concentration (see Appendix B).

Once the leaf-level fluxes are obtained, the third step is to upscale these leaf-level sources or sinks per unit volume to equivalent sinks or sources at each gridbox. For this, we make use of the plant area density vertical profile as well as the ratio of sunlit and shaded leaves at each vertical level. In the last step the LW profile within the canopy is updated with the re-calculated leaf temperature distributions. Afterward the radiation profiles as well as the vertically distributed temperature and scalar sinks and sources are passed on to the thermodynamic core of the LES model. Although it is possible in DALES account for a lag on stomatal response times (Sikma et al., 2018), for the sake of simplicity we assume an immediate stomatal response to the environmental conditions.

Appendix B contains a more detailed description on the canopy model implementation.

2.3. Observations

The observations used in the present study are part of the observational campaign GoAmazon2014/5. In particular, we employ 30-min averaged above-canopy observations of latent and sensible heat fluxes, net radiation, momentum and CO₂ fluxes at a height 48.2 from the 50-m tall K34 tower located at the Cuieiras Biological Reserve (2° 36' 32"S, 60° 12' 33"W) (Fuentes et al., 2016). An infrared gas analyzer (model LI-7500A, LI-COR Inc., Lincoln, Nebraska) was used to obtain the information needed to compute latent heat and CO₂ turbulent fluxes above the canopy. Additional observations on in-and-above canopy wind as well as momentum and temperature turbulent fluxes were collected during a field campaign conducted from March 2014 to January 2015. The K34 tower was instrumented with a vertical array of 9 sonic anemometers (model CSAT-3, Campbell Scientific Inc). Given the canopy height $h_c \sim 35$ m, heights of the array corresponded to $\frac{z}{h_c} = 0.2, 0.39, 0.52, 0.63, 0.70, 0.90, 1.00, 1.15$, and 1.38. Sonic anemometers recorded the three components of wind velocity (u, v, w) and sonic temperature T_s at 20 Hz frequency from which 30 min averages for wind speed and covariances $\overline{u'w'}, \overline{w'T'}$ were calculated. No detrending nor stationarity test was applied to the measurements, thus the previous should be considered raw covariances.

All previous observations correspond to the month of September 2014 and have been filtered to keep only clear-sky and shallow convective days. In addition, we used in Appendix B observations of photosynthetically active radiation (PAR, between 400 and 700 nm) collected near the Amazon Tall Tower Observatory (ATTO) (2° 8' 44"S, 59° 0' 17"W) during 2015. PAR was measured in a vertical profile inside the undisturbed canopy with energy sensors model SKE 510 from Skye Instruments. The sensors were mounted in 4 m long aluminum masts and collected data every minute from 29 September 2015 to 13 March 2016. Three sensors were installed as sensors facing up and three more sensors facing down at the south, east and west sides of the tower at 39 m. At the following heights and orientations one sensor facing up and another one facing down were installed: above the canopy; at the south side at a height of 33 m; at the west side at a height of 28 m; at the east side at a height of 22 m; at the south side at a height of 16 m; at the west side at a height of 11 m; at the east side at a height of 5 m.

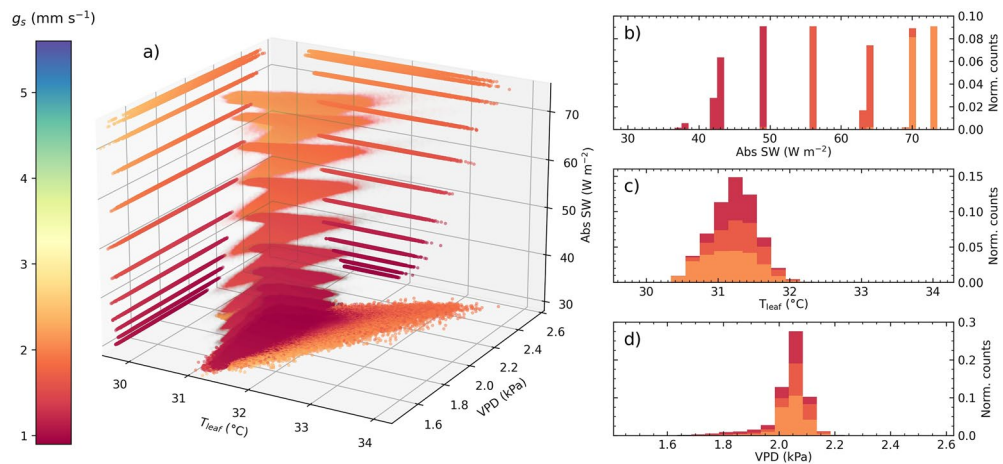


Figure 3. On the left, relation at 12:00 LT between instantaneous absorbed shortwave radiation (Abs SW) by vegetation on the vertical axis, Vapor Pressure Deficit (VPD) and leaf temperature (T_{leaf}) on the horizontal axes with the color-coded resulting water stomatal conductance (g_s) for all shaded leaves in the canopy in REF. On the right, the 3 figures show the normalized counts in the canopy for each variable associated to the stomatal conductance in color. The normalized count is defined as the number of canopy gridboxes with values within a certain bin divided by the total number of canopy gridboxes.

3. Results

Solving the leaf energy balance for sunlit and shaded levels independently at each vertical level in the canopy provides us with the unique opportunity to analyze the near-leaf-scale environment and related processes. In Figures 3 and 4 we display the vast range of environmental conditions taking place in our $3 \times 3 \times 3 \text{ m}^3$ discretization for shaded and sunlit leaves, respectively, and how that affects the resulting water stomatal conductance g_s . The stomatal conductance values in Figure 3 show that the photosynthesis in shaded leaves is low in general, and is limited, to a large extent, by the light availability. While VPD and leaf temperature play a small and no role, respectively, in modulating the leaf stomatal conductance in shaded leaves, the absorbed SW is the main factor limiting g_s . These findings are confirmed through the r correlation coefficients displayed on the upper half of Table 2. The limited ranges of absorbed SW radiation values in both Figures 3 and 4 reflect the still one-dimensional nature of the canopy radiative scheme. Despite this scheme being implemented at every canopy gridpoint, the homogeneously prescribed PAD vertical profiles combined with an equally horizontally homogeneous SW forcing at canopy top limits the variability of Abs SW. A more diverse distribution of Abs SW values is expected in cloudy or, particularly, partly cloudy conditions.

Figure 4 shows that leaf temperature and VPD influence the resulting stomatal conductance in sunlit leaves more than in shaded ones. With absorbed SW still regulating partly the leaf activity (see $r = 0.360$ in lower

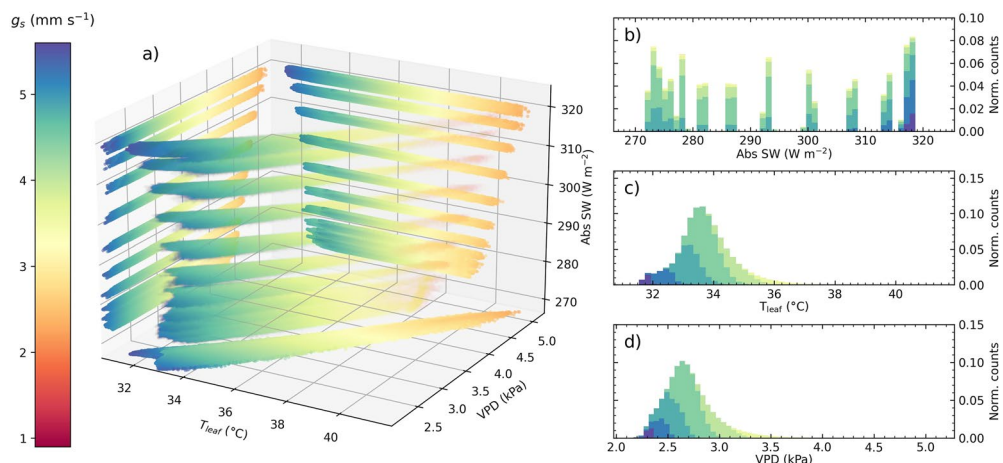


Figure 4. As in Figure 3 but for sunlit leaves.

Table 2

Pearson Correlation Coefficients r for the Leaf Level Variables Displayed in Figures 3 and 4 for Shaded and Sunlit Leaves on the Top and Bottom Tables, Respectively

	VPD	Abs SW	T_{leaf}
g_s	0.415	0.996	-0.006
T_{leaf}	0.207	0.023	
Abs SW	0.480		
g_s	-0.916	0.360	-0.934
T_{leaf}	0.922	-0.207	
Abs SW	-0.037		

half of Table 2), we now find that increasing T_{leaf} and VPD lead to lower g_s . The anticorrelation between VPD and g_s has been consistently reported under all environmental conditions (Fu et al., 2018; Massmann et al., 2019). An increase in T_{leaf} , however, may lead to larger or lower g_s depending on whether the initial leaf temperature is lower or higher than the optimal leaf temperature for photosynthesis (Jacobs et al., 1996). The A-gs model explicitly takes that behavior into account. Therefore, given the strongly negative correlation between g_s and T_{leaf} with $r = -0.934$ (lower half of Table 2), we conclude that in the simulated environmental conditions, typical of the Amazonian dry season, leaf temperature is above the optimal temperature at 12 LT. This agrees with studies like the one by Hernández et al. (2020) where they estimated the optimal temperature of three different tree species in Panama to be below 32°C for sunlit leaves. A comparison between Figures 3 and 4 provides information on the range over which leaf environment varies. The range in VPD and T_{leaf} is of about 1 kPa and 3.5°C respectively in shaded leaves, while

these ranges are about three times larger in sunlit leaves, of about 3 kPa and 9°C. We also find T_{leaf} and VPD to be highly correlated in sunlit leaves, while this is not the case in shaded ones (see bottom projections in Figures 3 and 4 and Table 2).

The changing environmental conditions were just shown to clearly affect stomatal conductance and its spatial variability. This, in turn, leads to heterogeneities in the local exchange of CO₂ and in the redistribution of available energy between sensible (SH) and latent (LE) heat fluxes both across height and the horizontal dimensions within the canopy. We show such variability in the horizontal cross-sections for the three sources/sinks at canopy top and bottom (Figure 5). Note that the sources and sinks displayed in Figure 5 are at the gridbox scale and, thus, per m³; and that they are termed local as they only represent the moisture, CO₂ and heat entering or leaving the atmosphere at each gridbox without considering the background turbulent flux. A first inspection shows the decreasing impact of wind with canopy depth: the canopy top shows stripe-like shapes oriented in the x direction, contrasting with the cell-like structures at canopy bottom. The three fluxes are characterized by a negative skewness as they show strong negative fluctuations, weaker in the case of SH. These negative fluctuations of the three fluxes are relatively stronger at the canopy top, where reductions in flux values are up to 35%, 20%, and 30% for LE, SH, and FCO₂, respectively. This is more visible in the lines plotted above and right of each cross section. The distance between minima visible in those lines are of at least 100 m, suggesting that these dynamics are influenced by scales larger than that

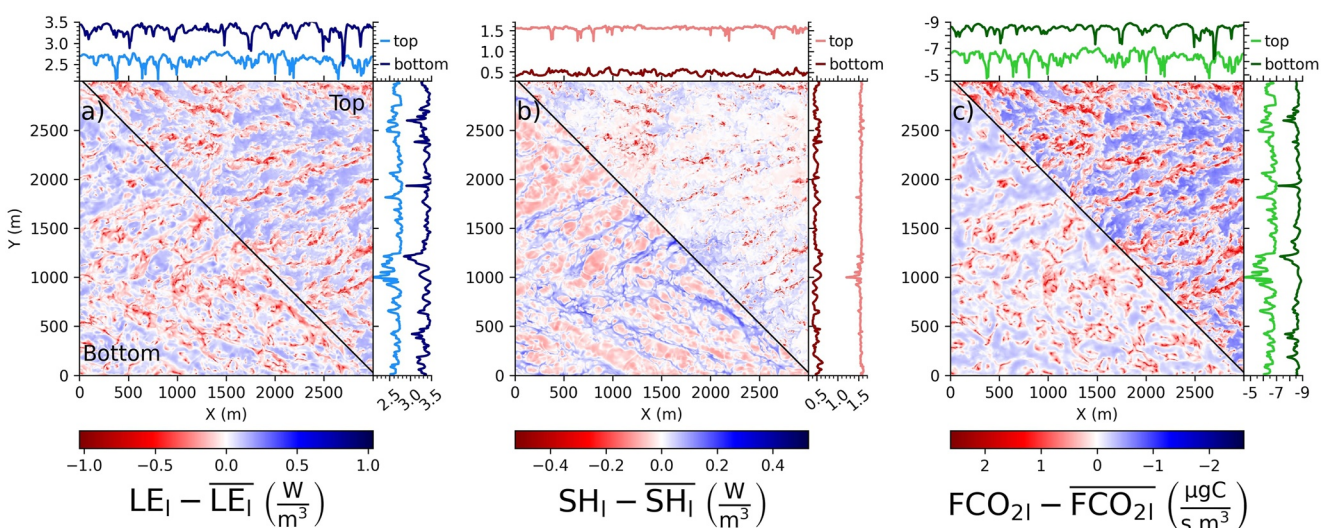


Figure 5. Instantaneous horizontal cross section at 12:00 LT of the canopy bottom ($z = 4.5$ m, lower left triangle) and canopy top ($z = 34.5$ m, upper right triangle) (a) showing the deviation from the slab average for latent heat local source, (b) sensible heat local source and (c) CO₂ flux local sink in REF. On the top and right of each subfigure, absolute values at canopy top and bottom along the $Y = 1,500$ m and $X = 1,500$ m lines, respectively.

of the canopy. Those lines also show a clear one-to-one match between the moisture and CO_2 fluxes due to their coupling through photosynthesis.

The heterogeneous and vertically varying sources and sinks of heat, moisture and CO_2 combined with the wind profiles have a direct impact on the state variables inside the canopy. Figure 6 shows the within and above canopy conditions for moisture, heat and CO_2 of a 1,000 m long cross section of the simulated domain. The canopy is characterized by more moist and CO_2 -rich air, and by temperature growing with canopy height and peaking above the level of maximum canopy density 1, as also found by Patton et al. (2016). Such temperature height-dependency is visible in the gray lines in left sub-figure for Figures 6a–6c. We define here the slab-average as the average of a quantity across both horizontal directions. The slab-averaged fluxes at leaf level for sunlit and shaded leaves are displayed on the right of each vertical cross-section. The resulting sink or source at the gridbox scale of these leaf-level fluxes was displayed in Figure 5 for two selected heights. All the slab-averaged vertical profiles of the leaf-level fluxes increase with canopy height, except for the lower levels of shaded SH_{leaf} . We find a stable stratification with potential temperature peaking a few meters below the canopy top. This will be further studied in Figure 10. The reader should note that the sunlit leaf-level fluxes are in the order of 3, 100 and 20 times larger than at shaded leaves for moisture, heat and CO_2 , respectively. The cross-sections allow us to visualize the turbulent structures that regulate the exchange between the canopy and the air above (Denmead & Bradley, 1985; LeMone et al., 2019; Shaw & Patton, 2003). A sweep transporting drier, colder and CO_2 -rich air downwards and penetrating the canopy is clearly visible at around $x = 700$ m. Similarly, an ejection of moist, warm and CO_2 -poor air upwards can be seen at $x = 550$. It is worth noting the role played by soil processes: there is a compensation of the CO_2 plant assimilation by soil respiration, leading to CO_2 concentration increasing near-surface. This is also found in the mean CO_2 profile as well as in the cross section in Figure 6c and will be further discussed in Figure 10.

An important aim of our research is the validation of the canopy model with observations and to demonstrate the need for comprehensive data sets. In the following figures we show an extensive validation of the four simulations described in Section 2.1 with the observations gathered during the GoAmazon2014/5 campaign. The radiative properties above the canopy are shown in Figure 7. There, we evaluate the use of RRTMG and the simpler Delta-Eddington radiation schemes. Both schemes perform similarly given the generally cloudless conditions and that aerosol effects are not considered. A convenient consequence of using the multilayer canopy model is that the effective canopy albedo varies dynamically in a realistic manner with the position of the sun, ranging from 0.165 to 0.115, because of the dependence of leaf scattering on solar angle. This variation also provides more realistic values for reflected shortwave radiation above the canopy as seen in Figure 7b. Here, the prescribed constant albedo for BULK is a compromise to mimic the reflected SW but shows clear deviations from observations of as much as 25 W m^{-2} at 12:00 LT.

We show in Figure 8 the turbulent fluxes for momentum, moisture, temperature and CO_2 both modeled and observed at a height of about 48 m, around 13 m above the top of the canopy. This figure helps to quantify the impact of explicitly simulating a multilayer canopy versus a bulk approach (Figure 2) in the above-canopy flow. Both REF and COARSE follow the observed mean values regarding u_* , LE and SH after the first hour of spinup. This suggests that both the dynamics of the flow within and near the canopy as well as the leaf energy balance that regulates the partitioning between sensible and latent heat flux are sufficiently well reproduced in the simulations to match above canopy conditions. However, the CO_2 flux in both REF and COARSE overestimates the increasing negative values after 10:00 LT. This finding points toward an insufficient replication of carbon processes in the model. Possible causes for the misrepresentation are of soil and ecophysiological origin: an underestimation of soil respiration or the overestimation of CO_2 uptake at leaf level. These issues reinforce the need to have detailed measurements for the photosynthesis dependence on PAR and on the carbon gradient between the leaf and surrounding air at short spatiotemporal scales (Vilà-Guerau de Arellano, Ney, et al., 2020). The BULK simulation shows larger discrepancies, falling outside the standard deviation, with the observed fluxes in Figures 8a–8c. This is particularly clear for u_* , demonstrating that a 0-order canopy representation cannot reproduce the canopy-induced modification to the turbulence (Finnigan et al., 2009), missing therefore important features of the canopy-atmosphere interaction such as the momentum transport by sweeping and ejection motions (Shaw & Patton, 2003). Interestingly, BULK suggests a different partition on the leaf energy balance given lower (larger) LE (SH) in the afternoon. The fluctuations at the first 30 min of the simulations are due to the spin-up needed by the model to fully develop turbulence.

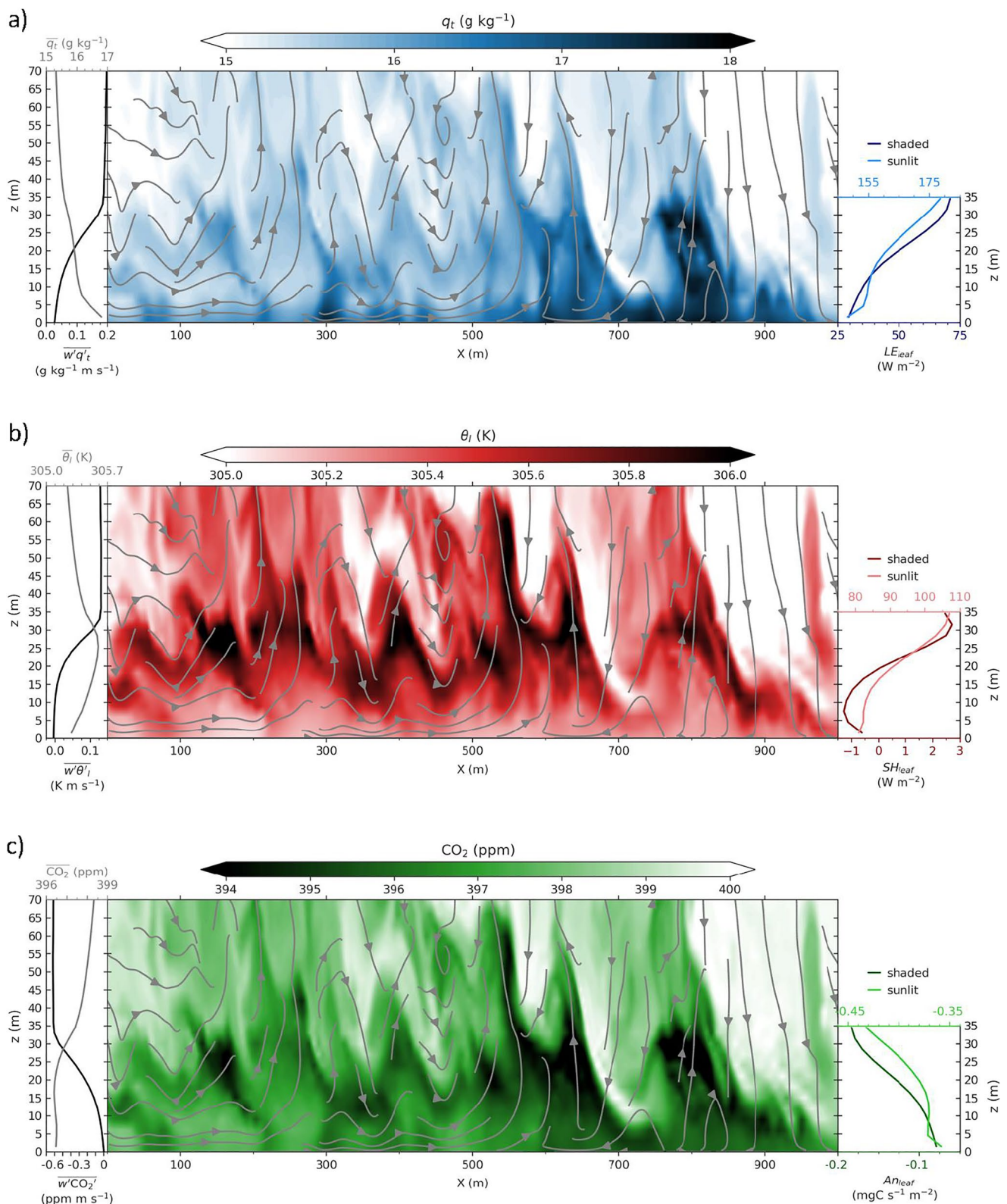


Figure 6. Instantaneous vertical cross sections of a domain subset of REF at 12:00 LT of the boundary layer lowest 70 m displaying the instantaneous fields for specific humidity q_t (a), liquid potential temperature θ_l (b) and CO_2 concentration (c) in color shades. Wind direction is shown in gray streamlines. On the left of each cross section, slab-average values of the shown variable in gray and of the associated turbulent flux in black. On the right of each cross section, slab-average values of the associated flux at leaf level for shaded (dark) and sunlit (light) leaves. Note that the canopy is present only up to 34.5 m.

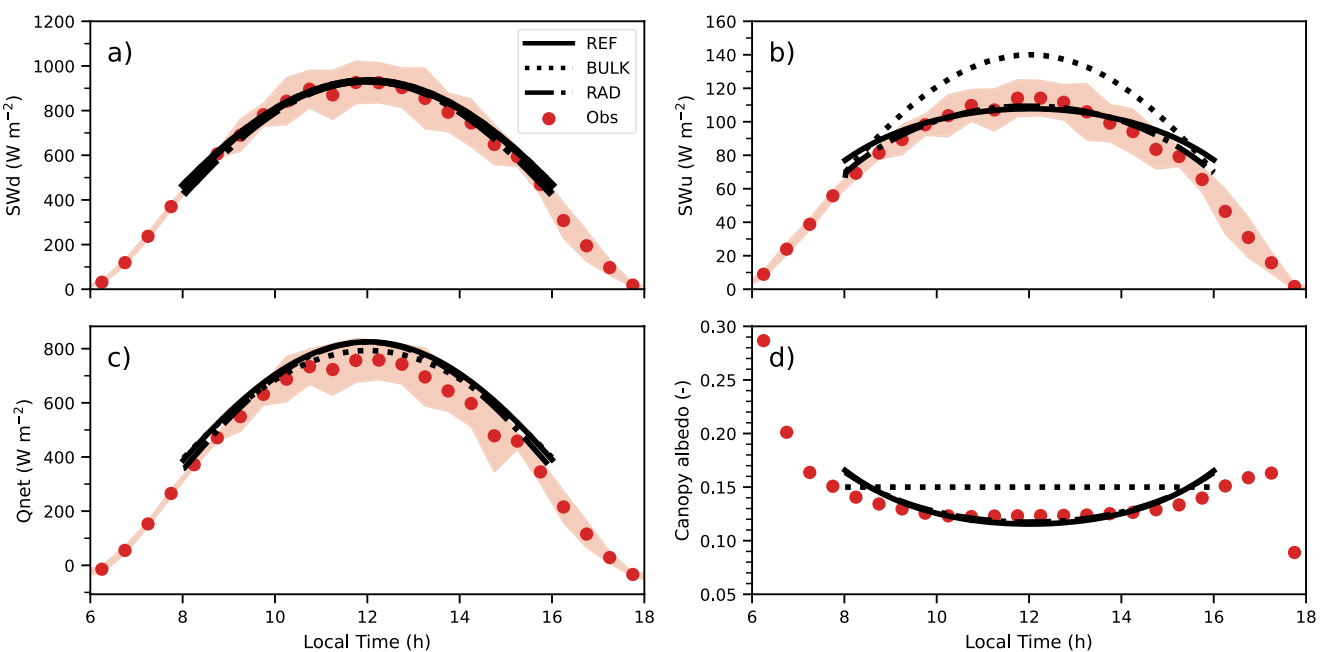


Figure 7. (a) Time series of slab-averaged downwards shortwave radiation SWd, (b) upwards shortwave radiation SWu, (c) net radiation Qnet, and (d) resulting canopy albedo above canopy top for the REF (full line), BULK (dotted) and RAD (dash-dotted) experiments. Observations are shown by the red dots, with the red shade width being two times the standard deviation across the sampled days.

The vertical distribution of the heat and momentum turbulent fluxes inside the canopy at three selected times is further studied in Figure 9. The lack of observations with sufficient vertical resolution does not allow the validation of other turbulent fluxes, that are therefore shown in Appendix C. The discrepancies in Figure 9 vertical profiles between BULK and other simulations in above-canopy fluxes shown in Figure 8 are due to an unrealistic description of the turbulent fluxes at the canopy-atmosphere interface. Using a multilayer canopy, both REF and COARSE profiles show the benefit of solving turbulence explicitly in order to represent, at least qualitatively, the typical shape and inflection point in fluxes below canopy top (Finnigan et al., 2009). The COARSE experiment shows a good fit to momentum flux observations with deviations from the mean below the standard deviation. However, in-canopy $\overline{w'\theta'}$ observations show that COARSE overestimates the heat fluxes below canopy top, even if most of the flux is explicitly resolved, by as much as 0.05 K m s^{-1} . The above canopy $\overline{w'\theta'}$ observation variability at 13 LT is too large to assess whether REF or COARSE are a closer representation of the flux. The reader should also note the large variability in above-canopy momentum flux observations. BULK is shown to underestimate the momentum flux at every level above the canopy and misses completely its logarithmic growth above the canopy top.

The main state variables inside and above the canopy at the same selected times are depicted in Figure 10. Observed moisture and temperature show here larger relative discrepancies. Interestingly, the results reported by Ma and Liu (2019) in their LES experiments showed qualitatively similar disagreements with observations in a sparse orchard. Although Figure 6 showed REF to be weakly stable within the canopy up to the height of maximum PAD, none of the experiments reproduces accurately the strength of this thermally stable layer inside the canopy and underestimate the air temperature below canopy top by about 3.5 K . The disagreement is also large in the moisture profiles with differences between experiments and observations of as much as 6 g kg^{-1} in the mid-canopy. Ma and Liu (2019) suggested the large-scale motions and advection as the source for the moisture underestimation inside the canopy. The wind profiles are remarkably well reproduced both by REF and COARSE in terms of the shape, logarithmic above the canopy and exponential from canopy-top down into the canopy, as well as in magnitude. The limitations of BULK are apparent there: BULK overestimates windspeeds just above the canopy by as much as 2.5 m s^{-1} as it was suggested by its underestimated momentum flux $\overline{u'w'}$ in Figure 9. The CO₂ concentration profiles reproduce to a certain extent the unique CO₂ observations above the mid-canopy with deviation from the observed mean below 10 ppm. The little vertical variability of the in-canopy

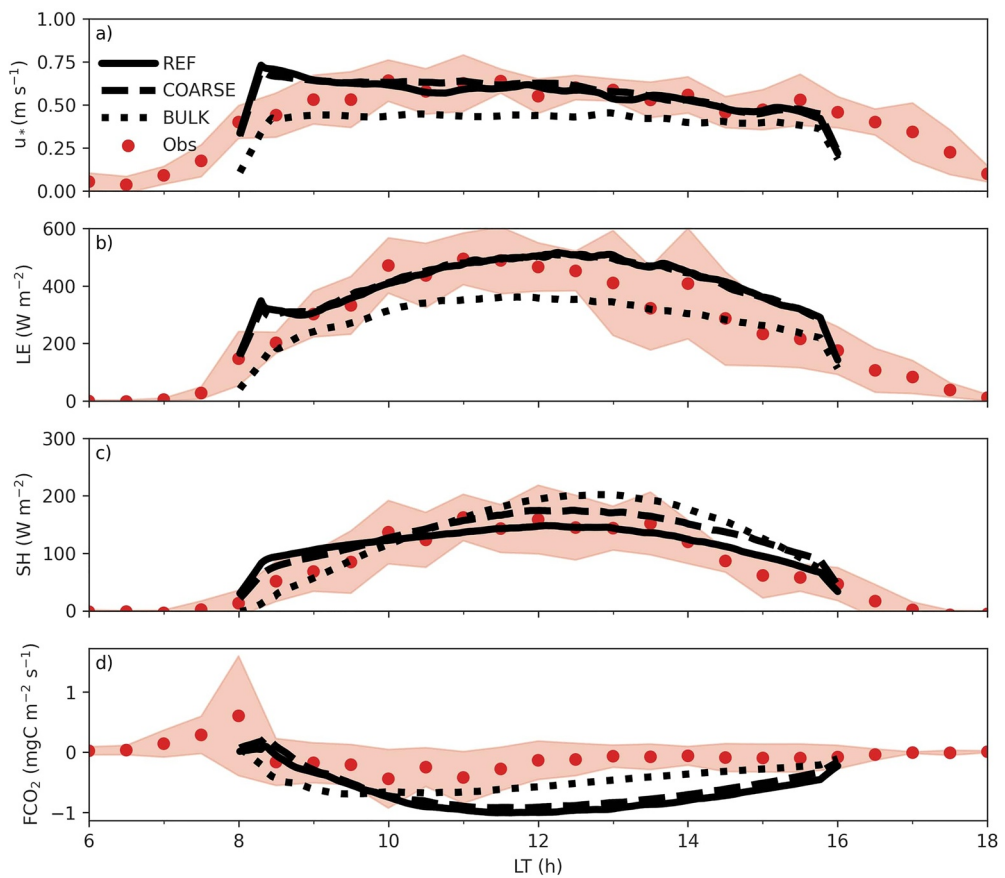


Figure 8. (a) Time series of slab-averaged friction velocity u_* , (b) latent heat flux LE, (c) sensible heat flux SH, and (d) CO_2 flux above canopy top for REF (full lines), COARSE (dashed) and BULK (dotted) experiments. A moving 30-min average was done on all modeled fluxes. Observations are shown by the red dots, with the red shade width being two times the standard deviation across the sampled days. All simulations show fluxes at the closest vertical level to the observation height of 48.2 m, except for BULK, where we plot the closest level to $48.2 - d$, with d the displacement height.

CO_2 profiles suggests an overestimation of the mixing inside the canopy. For near-surface observations, however, large discrepancies of as much as 30 ppm are found, reinforcing the idea that soil respiration is not accurately represented in the numerical experiments.

4. Discussion

The results shown above suggest several points for discussion and further work in the field of canopy-atmosphere interactions at small spatiotemporal scales, both in the modeling and observational aspects. As for the observations, there is currently a clear lack of data concerning both the radiative as well as the ecophysiological processes inside the vegetated canopy in combination with usual state meteorological variables such as wind, temperature and specific humidity. Long term co-located measurements of all these processes would be the end goal, while intensive and short campaigns would already be of use for the modeling community. As coupled models advance in the explicit solving of those processes, the availability of data sets with high-spatiotemporal resolution against which numerical experiments can be validated in terms of, for example, upwards and downwards radiation, leaf temperatures or stomatal conductance, is indispensable (Helbig et al., 2021; Vilà-Guerau de Arellano, Ney, et al., 2020). In the case of leaf measurements such as leaf-level fluxes, leaf temperature and stomatal conductance, there is plenty of data on laboratory conditions. However in-canopy observations of the previous variables, where all atmospheric and biologic processes take place simultaneously, are much scarcer.

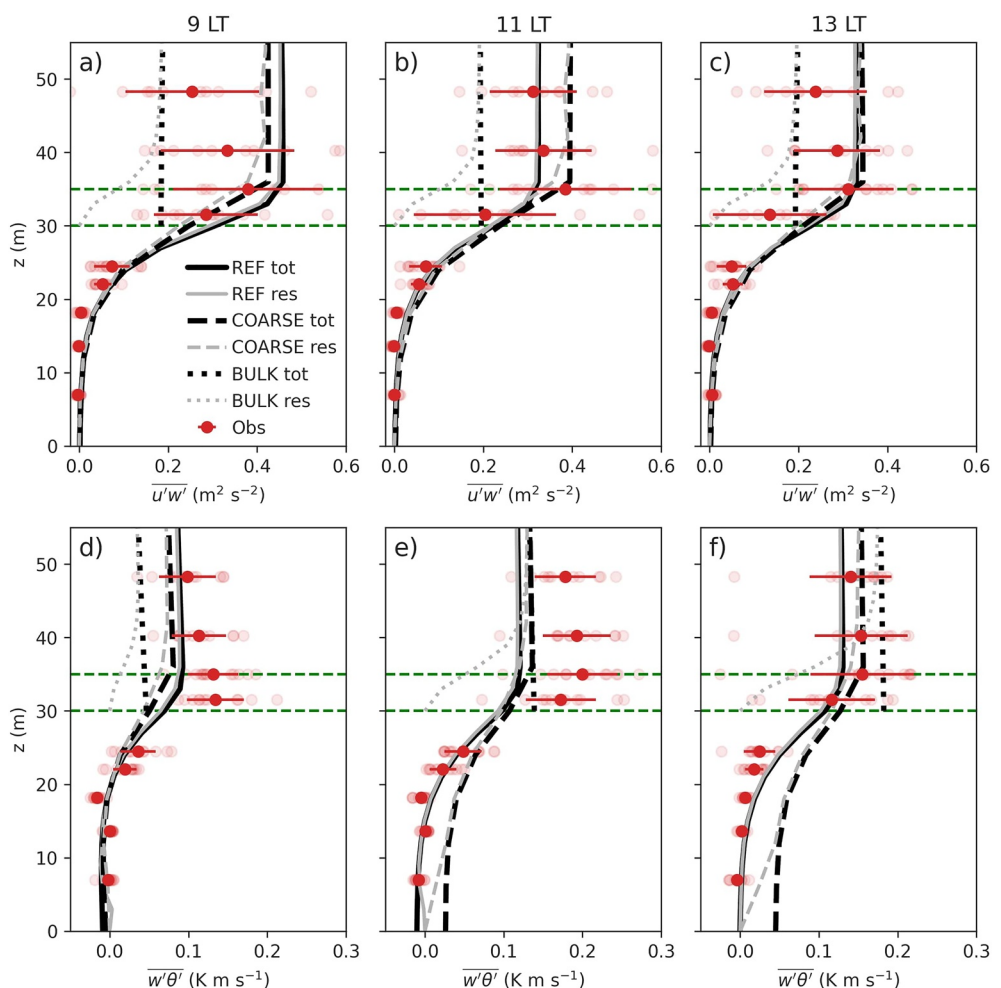


Figure 9. Slab 30-min averaged vertical profiles within and above the canopy of the turbulent momentum flux $\overline{u'w'}$ (top) and heat flux $\overline{w'\theta'}$ (bottom) at 9:00 LT (left), 11:00 LT (center) and 13:00 LT (right) for REF (full line), COARSE (dashed) and BULK (dotted) experiments. Black and gray lines show the total (tot) and resolved (res) fluxes, respectively. Observations are given by the red dots, with the red shade width being two times the standard deviation across the sampled days. The green horizontal lines indicate the observed lowest and highest tree tops in the canopy. Note that the vertical coordinate is $z + d$ for BULK.

Results in Figures 8 and 10 showed that the numerical experiments miss partly some of the in-canopy processes affecting moisture and carbon, particularly near the ground. Related to the above mentioned observation scarcity, these discrepancies point to the need to refine the model representations of soil and ecophysiological processes, where real-world data availability is crucial. At the same time our comprehensive numerical simulations in the upper-part and above the Amazonian rain-forest are useful to advance the understanding on how the inertial sublayer and roughness sublayer influence the measurements of mean state variables, variances and fluxes (Dias-Júnior et al., 2019) and they further contribute towards more realistic canopy representations when assessing the role of topography on surface flux measurements (Chamecki et al., 2020).

The finding that carbon processes need to be better represented in our model suggests that the exchange of other related chemical species between the canopy and the atmosphere may not be correctly represented in current models. The most direct example of a related flux is the evapotranspiration due to the coupled water and carbon exchange during plant photosynthesis. Comparing modeled and measured fluxes of stable isotopologues, helpful to discriminate NEE contributions between plant assimilation and soil respiration, could help in shedding light on the in-canopy carbon processes. Although it requires further studies, such isofluxes can be already observed

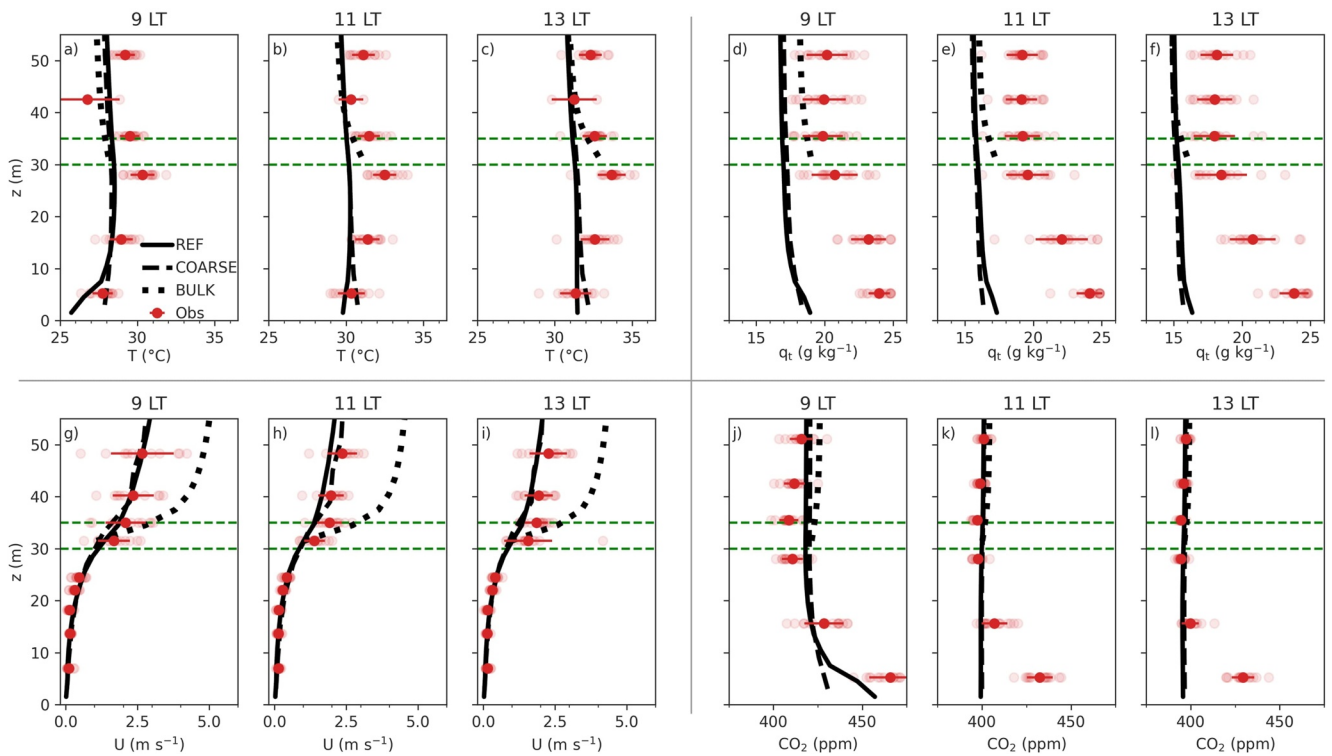


Figure 10. As in Figure 9 but for (a–c) temperature T , (d–f) specific humidity q_t , (g–i) horizontal wind U , and (j–l) CO_2 concentration.

(Griffis, 2013) and modeled (Vilà-Guerau de Arellano et al., 2019), and are susceptible to show similar biases when using our canopy scheme. Similarly, ozone and biogenic volatile organic compound (BVOC) or isoprene fluxes, giving information on the state of the photosynthesizing leaves, may suffer from related biases as the ones shown here for carbon processes. This further reinforces the need for integrated and comprehensive studies combining both the physics and the chemistry of the canopy.

The in-canopy radiative transfer scheme is shown in Figure 7 to provide reliable SW radiation at the canopy top. In addition, Figure B1 shows acceptable results for the downwelling PAR component inside the canopy. Although the lack of GoAmazon2014/5 observations at the time of the numerical experiments hinders the identification of representation errors, the available data suggests that a multiband radiative transfer scheme, including the spectral dependency of leaf-radiation interactions, would further improve the absorbed PAR and in-canopy profiles. In that respect, current radiation measurements and modeling initiatives to include a better wavelength dependence show the convenience of higher detail on the spectral radiative transfer (Moon et al., 2020). A further improvement in the representation of radiation would imply the addition of three-dimensional radiative effects both above the canopy, particularly important in partly cloudy conditions, and inside the canopy to account for horizontal heterogeneities in vegetation. Despite the computational as well as conceptual challenge this implies, we find it relevant since the canopy models can only be used as an horizontally homogeneous approximation of real-life conditions as long as those three-dimensional processes are not incorporated.

Finally, the relatively small domain currently possible in the present study, on the order of 10 km, also poses a limitation in the represented scales, as it is often argued in LES studies. The high resolution, finer than 10 m, needed to start resolving the canopy processes is an additional constrain for the computational cost involved. Therefore, as also suggested by Ma and Liu (2019), the results showed here may benefit from having a representation of scales larger than the simulated domain. A possible solution currently feasible is to embed simulations like the ones presented here in larger scale models that account for synoptic and mesoscale variability, or to perform less idealized simulation with realistic and time-varying lateral forcings.

5. Conclusions

In this study, we present numerical experiments explicitly resolved from the atmospheric boundary layer scales down to nearly leaf level scales in the Amazonian rainforest. To that end, we implemented a single-column multilayer canopy model in DALES. Verification is carried out with a comprehensive observational data set gathered in and above the canopy during the month of September 2014, representative of a fair weather day, and the model is validated it by reproducing a day with atmospherically unstable and typical fair weather Amazonian conditions. To our knowledge, this is the first validation of in-canopy carbon processes in a LES model. Provided with the needed radiative and thermodynamic forcings by the LES model, the multilayer canopy scheme performs the radiative transfer calculations through the canopy, the leaf energy balance for sunlit and shaded leaves independently at each vertical level and the conversion of the resulting leaf level fluxes to grid-scale sources and sinks. We systematically constructed numerical experiments to answer our research questions in terms of needed resolution, complexity of radiation transfer scheme and overall impact of the multilayer canopy scheme. Key in the validation process was the use of an extensive data set of meteorological observations inside and above the vegetated canopy gathered during the GoAmazon2014/5 campaign.

The use of a very fine resolution of up to $3 \times 3 \times 3 \text{ m}^3$ allowed us to display the large environmental variability in terms of radiation, moisture and temperature present at the leaf scale and the overall impact these factor exert on stomatal conductance. This is a key variable as it regulates the exchange of water and CO_2 between the canopy and the atmosphere and, consequently, the leaf temperature and the related canopy sink or source of heat. The in-canopy environmental variability was found to be about three times larger for sunlit than shaded leaves in terms of vapor pressure deficit and leaf temperature. At the canopy scale the wind was found to drive the formation of striped shapes on the local sources or sinks of heat, moisture and CO_2 at canopy top, while at the lower canopy cell-like structures were dominant. Due to the used domain of about $3 \times 3 \times 2.8 \text{ km}^3$ where the full turbulent ABL is included we identified typical structures of the exchange between the canopy and the atmospheric boundary layer such as ascending ejections of moist, warmer and CO_2 -poor air and descending sweeps with dry, colder and CO_2 -rich air. The vertical variability of horizontally averaged leaf level fluxes was also studied differentiating between fluxes of sunlit and shaded leaves. There, we found the sunlit leaf-level fluxes of moisture, heat and CO_2 to be around 3, 100, and 20 times larger, respectively, than the shaded leave-level fluxes at the time of maximum solar insolation.

The complete observational data set was used to validate above and inside canopy meteorological variables. Above-canopy radiation and turbulent fluxes were shown to agree to a large extent between observations and simulations, with some disagreements in the CO_2 flux above canopy starting in the late morning. Results showed that any of the canopy multilayer descriptions improves the traditional bulk canopy representation. A finer spatial resolution was shown to be beneficial for the representation of these variables. Concerning the in-canopy variables, turbulent fluxes of momentum and heat showed overall the benefit of using a multilayer canopy compared to typical bulk canopy schemes. Similarly, the representation of state variables such as temperature and wind inside the canopy was improved by the multilayer canopy experiments, while humidity and CO_2 shown some disagreements particularly at the low canopy.

We finally discussed some of the issues encountered during the study such as the scarcity of complete data sets describing the radiation, thermodynamics and ecophysiology of the boundary layer-canopy continuum. We also described the limitations in our numerical experiments, namely: on the soil and ecophysiological processes driving the moisture and carbon distribution; on the in-canopy broad-band radiative transfer scheme; and on the lack of complete observation sets covering canopy and meteorological processes. Based on these limitations we also suggested directions for further improvement in representing the interactions at the sub-daily scale between the canopy and the atmospheric boundary layer.

Appendix A: Modifications to Original Case Setup

Table A1 and Figure A1 show the new or modified settings and the modified initial vertical profiles, respectively, with respect to the original case described in Vilà-Guerau de Arellano, Wang, et al. (2020). All profiles above 500 m and wind profiles are not shown since they are identical to Vilà-Guerau de Arellano, Wang, et al. (2020). The prescribed Plant Area Density profile is shown in Figure 1.

Table A1
New or Modified Variables in the Numerical Experiment REF With Respect to Those in Vilà-Guerau de Arellano, Wang, et al. (2020)

Parameter	Explanation	Value
C_d	Canopy drag coefficient	0.15
lclump	Effect of leaf clumping on radiation	1 (=no effect)
leaf_eps	Leaf LW emissivity	0.95
llength	Leaf/shoot length	0.1 m
lwidth	Leaf width/shoot diameter	0.02 m
n canopy	Number of canopy layers	12
R_{10}	Soil respiration at 10°C	0.044 mg CO ₂ m ⁻² s ⁻¹
transpiretype	Type of leaf transpiration (1 = hypostomatous, 2 = amphistomatous, 1.25 = hypostomatous with some transpiration through cuticle)	1
σ	Leaf scattering coefficient	0.45
surf_albedo	Ground albedo	0.15

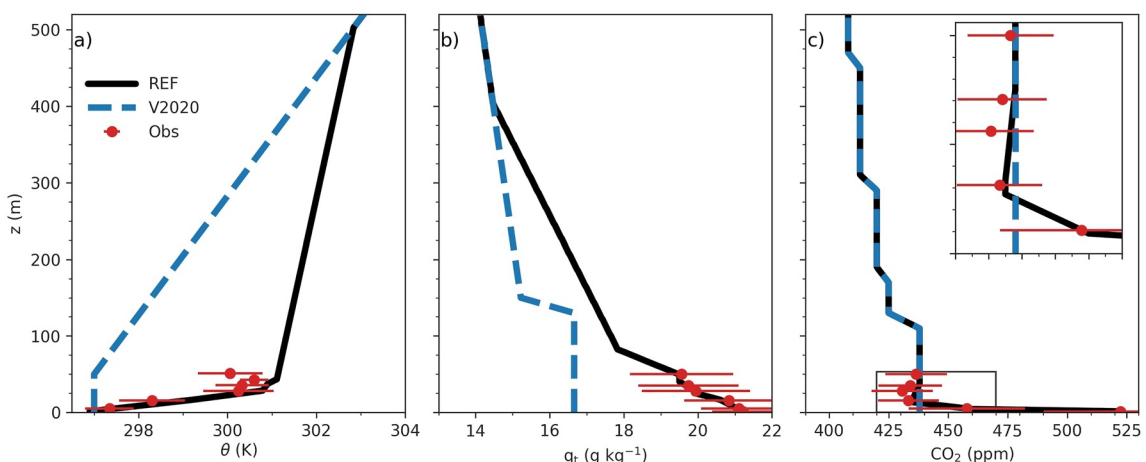


Figure A1. Lower 500 m of the initial profiles prescribed for the REF experiment (full black line) and the experiment in Vilà-Guerau de Arellano, Wang, et al. (2020) (V2020, blue dashed line) and the inside and above tower observations corresponding to September 2014 (red dots).

Appendix B: Description of the Multilayer Canopy Model

B1. General Description

This appendix gives further details on the implementation of the multilayer canopy energy balance (eb) in DALES. The implemented code requires some information on the canopy structure and characteristics and, combined with radiation transfer computations, it provides the in-canopy updated radiation profiles and sources of turbulent heat flux (SH), latent heat flux (LE) and CO₂ flux (FCO₂) per canopy layer. In between steps are the radiative transfer calculations within the canopy, the leaf energy balance for sunlit and shaded leaves per vertical level where the A-gs model is used to obtain leaf stomatal conductance, and the upscaling of the heat, moisture and CO₂ fluxes from leaf to gridbox level.

We based a significant part of our implementation in the work by Patton et al. (2016), with some substantial differences, namely: a different canopy radiative transfer model, the use of A-gs for stomatal conductance calculation that adds a carbon dependency to plant photosynthesis activity, the incorporation of CO₂ leaf exchange and, consequently, CO₂ fluxes, and the calculation and use of a canopy effective albedo.

B2. SW Radiative Transfer and LW Into Leaves

The radiation profiles are first calculated by the chosen radiation scheme in DALES (see Table 1) down to the surface as if no canopy was present. In the first step of canopy-eb, the direct and diffuse SW radiation values at the canopy highest gridpoint are taken as input as well as the surface albedo. The in-canopy radiation scheme calculates absorbed PAR at each vertical level. Additional calculated variables are: PAR absorbed at each canopy layer by sunlit and shaded leaves separately, fraction of sunlit leaves at each canopy layer f_{SL} , and effective canopy albedo. The direct PAR absorbed by sunny leaves is calculated here for three leaf angles, and is later averaged using Gaussian integration methods to account for a leaf spherical distribution (Goudriaan & van Laar, 1994). The reader is referred to Goudriaan and van Laar (1994) and Pedruzo-Bagazgoitia et al. (2017) for further details on the canopy radiation scheme.

Given that no detailed in-canopy radiation measurements were available during the GoAmazon2014/5 campaign, we compared the SW radiative transfer performed by DALES in our experiments REF and RAD (Table 1) against a set of observations gathered during October 2015. Figure B1 shows both the calculated in-canopy profiles and the values at the observed heights and orientation. The observations obtained are a useful resource to assess the realism of the radiative scheme even if the month and year differ between the observations and the numerical experiments. Figure B1 shows that the radiative scheme performs satisfactorily for calculating the downwards radiation profiles as well as the upwards SW above the canopy. Regarding the upwards radiation components, however, the coarse relationship relating $\text{PAR} = 0.5 \text{ SW}$ no longer holds (see differences between red dots and above-canopy blue dots) due to the varying transmissive and scattering properties of leaves across the shortwave range of the electromagnetic spectrum. Since only SW measurements were available during the period on which

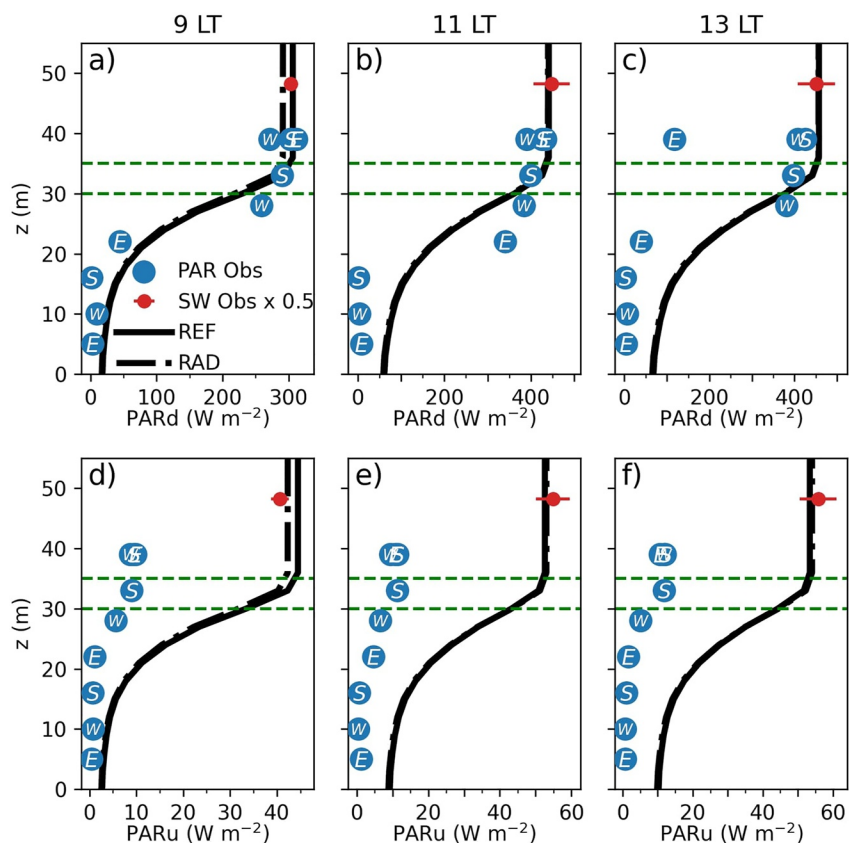


Figure B1. (top) Vertical profiles of in-canopy downwards and (bottom) upwards slab-averaged PAR, calculated as $\text{PAR} = 0.5 \text{ SW}$ for REF (full line) and RAD (dashed-dotted line) experiments at three selected times: 9 (left), 11 (center) and 13 (right) Local time. The red dots denote the PAR obtained from measuring SW and approximating $\text{PAR} = 0.5 \text{ SW}$ during selected days in September 2014, while the blue dots are actual PAR observations but obtained during a different period, that is, October 2015 (see Section 2.3). The letter inside each blue dot shows the orientation of each observation.

our numerical experiments are based, the canopy properties were adjusted (Table A1) to better fit those values, and show larger discrepancies with the later measured in-canopy upwards PAR. This result also suggests the need to compute the radiative transfer for several spectral bands in further work to better mimic the interactions between light and leaves.

B3. Leaf Energy Balance

The leaf energy balance is calculated independently for each vertical canopy level and for shaded and sunlit leaves. It assumes that leaves reach thermal equilibrium immediately. Therefore, we neglect canopy heat storage. The motivation to do this is the large uncertainty and inter-plant variability in the properties required for the calculation of heat storage such as biomass volume per gridbox or vegetation specific heat. A small variation in these values would lead to large changes in heat storage and, consequently exaggerated changes in air temperature tendencies. The procedure to compute leaf temperature is based on an iterative algorithm starting with two leaf temperature T_{leaf} guesses above and below the air temperature and using a bisection method where it is assumed that the function leading from T_{leaf} to the residual energy ($Res = SW_{in} + LW_{in} - LW_{out}(T_{leaf}) - SH(T_{leaf}) - LE(T_{leaf})$) is linear between the current two T_{leaf} guesses.

The stomatal CO_2 conductance at leaf level g_c is calculated following A-gs (Jacobs & de Bruin, 1997; Vilà-Guerau de Arellano et al., 2015) at each iteration. Afterward, the leaf-boundary layer conductance for heat g_{bl} is calculated following Leuning et al. (1995) and Nikolov et al. (1995). Then, the SH and LE fluxes at leaf level are computed, considering also if the leaves are amphistomatous or hypostomatous. The formulas for the leaf-level fluxes read:

$$SH = 2g_{bl} \rho cp (T_{leaf} - T_{air}) \quad (B1)$$

$$LE = \tau Lv \frac{VPD}{\frac{1}{1.075g_{bl}} + \frac{1}{1.6g_c}} \quad (B2)$$

where cp is the specific heat of air, T_{air} the air temperature, VPD is the vapor pressure deficit and $\tau = 1$ for hypostomatous leaves and $\tau = 2$ for amphistomatous. The 1.6 factor next to g_c accounts for the ratio between the molecular viscosity of water to that of carbon dioxide.

LW_{out} is calculated using Stefan-Boltzmann's equation with T_{leaf} and assuming a leaf emissivity of $\epsilon = 0.95$. Once the iteration process converges, T_{leaf} , LW_{out} , LE and SH, g_{bl} are stored, and the CO_2 flux is calculated following Goudriaan and van Laar (1994) by:

$$FCO_2 = -\tau \frac{CO_2^{air} - ci}{\frac{1}{g_c} + 1.4 \frac{1}{1.075g_{bl}}} \quad (B3)$$

Here ci is plant internal carbon concentration and is dependant on air temperature and CO_2 concentration, VPD, and mesophyll conductance (Vilà-Guerau de Arellano et al., 2015). The lag on stomatal regulation and on ci is implemented and applied at leaf level. It is however not used for the present study.

B4. Upscale From Leaf Flux to Gridbox Source

The fluxes calculated at leaf level are dependent on the canopy level and whether the leaves are sunlit or shaded. Therefore, a transformation is needed from leaf-level fluxes SH, LE and FCO_2 into sources/sinks of θ , qt and CO_2 , respectively, at the gridbox scale. Taking the heat flux as example, this is done for vertical level k by:

$$S_{SH}(k) = PAD(k)(fSL(k) SH_{sunleaf}(k) + (1 - fSL(k)) SH_{shadleaf}(k)) \quad (B4)$$

and similarly for LE and FCO_2 . S_{SH} is the source/sink of sensible heat, $SH_{sunleaf}$ and $SH_{shadleaf}$ the SH at leaf level for sunlit and shaded leaves, respectively, $PAD \left[\text{m}_{leaf}^2 / \text{m}_{air}^3 \right]$ the plant area density and fSL the fraction of sunlit leaves. This provides sources and sinks to be integrated in the model.

Appendix C: Moisture and Carbon Fluxes Inside the Canopy

Figure C1 shows the turbulent fluxes of both moisture and carbon inside following Figure 9. However, no vertically detailed observations were available to compare against these simulated quantities.

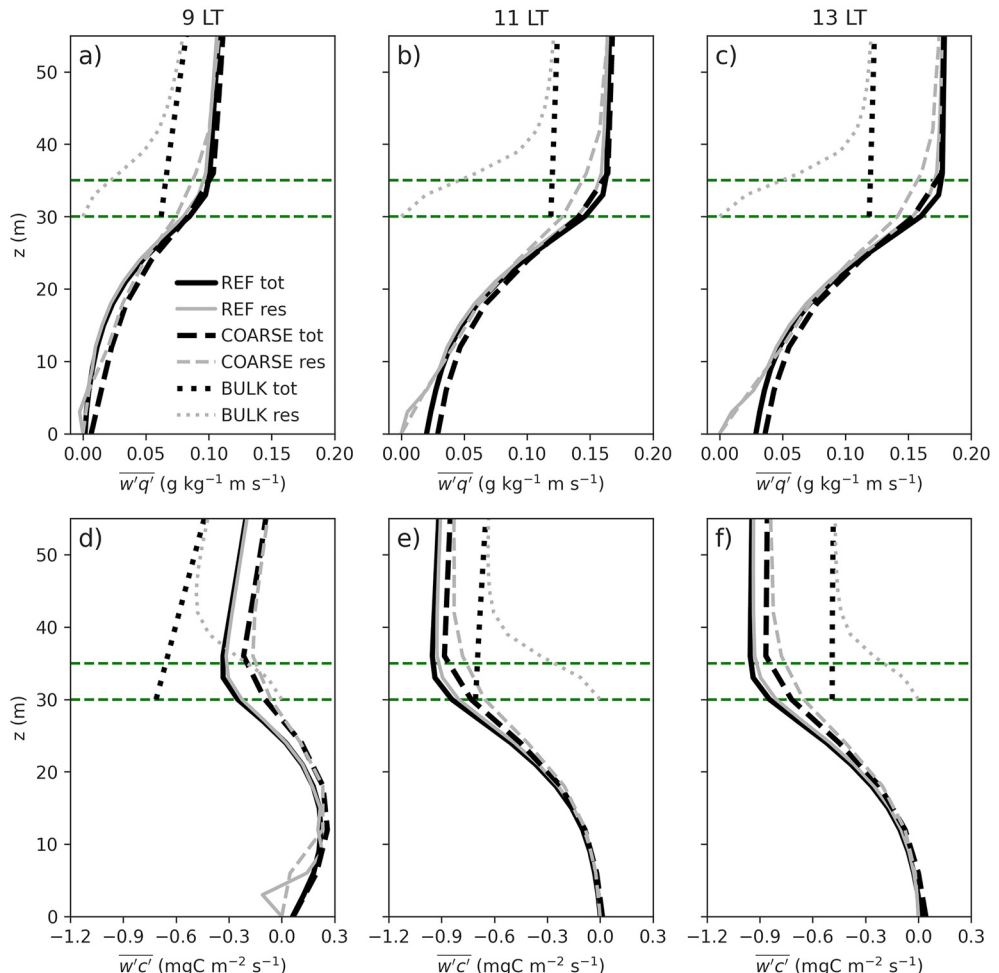


Figure C1. Slab 30-min averaged vertical profiles within and above the canopy of the turbulent moisture flux $\overline{w'q'}$ (top) and carbon flux $\overline{w'c'}$ (bottom) at 9:00 LT (left), 11:00 LT (center) and 13:00 LT (right) for REF (full line), COARSE (dashed) and BULK (dotted) experiments. Black and gray lines show the total (tot) and resolved (res) fluxes, respectively. The green horizontal lines indicate the observed lowest and highest tree tops in the canopy. Note that the vertical coordinate is $z + d$ for BULK.

Data Availability Statement

The exact code version of the DALES model used together with the input files needed for each of the experiments showed in this manuscript can be found in <https://doi.org/10.5281/zenodo.6582455> (Pedruzo-Bagazgoitia, 2022a). The most recent published version of DALES is available here: <https://doi.org/10.5281/zenodo.4604726> (Arabas et al., 2022). The scripts and observational data leading to the figures shown in the manuscript are available at <https://doi.org/10.5281/zenodo.6582524> (Pedruzo-Bagazgoitia, 2022b).

Acknowledgments

We would like to thank the comments by three anonymous reviewers that helped to improve the final version of the manuscript. This work was carried out on the Dutch national e-infrastructure with the support of SURF Cooperative (NWO project on Exact and Physic Science 2019.044). We would also like to thank Dr. Susanne Wiesner for technical support in obtaining the experimental observations. The U.S. Department of Energy supported the field studies as part of the GoAmazon project (Grant SC0011075). Fundação de Amparo à Pesquisa do Estado de São Paulo (FAPESP) and Fundação de Amparo à Pesquisa do Estado do Amazonas (FAPEAM) funded the Brazilian component of the field studies. The authors acknowledge the support from the Central Office of the Large-Scale Biosphere-Atmosphere Experiment in Amazonia (LBA), the Instituto Nacional de Pesquisas da Amazonia (INPA), and the Universidade do Estado do Amazonia (UEA). The work was conducted under 001030/2012-4 of the Brazilian National Council for Scientific and Technological Development (CNPq). EGP is supported by the National Center for Atmospheric Research, which is a major facility sponsored by the National Science Foundation under Cooperative Agreement No. 1852977.

References

Andreae, M. O., Afchine, A., Albrecht, R., Holanda, B. A., Artaxo, P., Barbosa, H. M. J., et al. (2018). Aerosol characteristics and particle production in the upper troposphere over the amazon basin. *Atmospheric Chemistry and Physics*, 18(2), 921–961. <https://doi.org/10.5194/acp-18-921-2018>

Arabas, S., Axelsen, S., Attema, J., Azizi, V., Beets, C., Boeing, S. J., et al. (2022). dalesteam/dales: Dales 4.4 [Dataset]. Zenodo. <https://doi.org/10.5281/zenodo.6675720>

Barbaro, E., Vilà-Guerau de Arellano, J., Krol, M. C., & Holtslag, A. A. M. (2013). Impacts of aerosol shortwave radiation absorption on the dynamics of an idealized convective atmospheric boundary layer. *Boundary-Layer Meteorology*, 148(1), 31–49. <https://doi.org/10.1007/s10546-013-9800-7>

Bonan, G. B., Patton, E. G., Finnigan, J. J., Baldocchi, D. D., & Harman, I. N. (2021). Moving beyond the incorrect but useful paradigm: Reevaluating big-leaf and multilayer plant canopies to model biosphere-atmosphere fluxes – A review. *Agricultural and Forest Meteorology*, 306, 108435. <https://doi.org/10.1016/j.agrformet.2021.108435>

Boulton, C. A., Lenton, T. M., & Boers, N. (2022). Pronounced loss of Amazon rainforest resilience since the early 2000s. *Nature Climate Change*, 12(3), 271–278. <https://doi.org/10.1038/s41558-022-01287-8>

Brunet, Y. (2020). Turbulent flow in plant canopies: Historical perspective and overview. *Boundary-Layer Meteorology*, 177(2), 315–364. <https://doi.org/10.1007/s10546-020-00560-7>

Brutsaert, W. (1975). On a derivable formula for long-wave radiation from clear skies. *Water Resources Research*, 11(5), 742–744. <https://doi.org/10.1029/WR011i005p00742>

Cescatti, A., & Niinemets, Ü. (2004). Leaf to landscape. In W. K. Smith, T. C. Vogelmann, & C. Critchley (Eds.), *Photosynthetic adaptation: Chloroplast to landscape* (pp. 42–85). Springer New York. https://doi.org/10.1007/0-387-27267-4_3

Chamecki, M., Freire, L. S., Dias, N. L., Chen, B., Dias-Junior, C. Q., Machado, L. A. T., et al. (2020). Effects of vegetation and topography on the boundary layer structure above the Amazon forest. *Journal of the Atmospheric Sciences*, 77(8), 2941–2957. <https://doi.org/10.1175/JAS-D-20-0063.1>

Cuypers, J. W. M., & Duynkerke, P. G. (1993). Large eddy simulation of trade wind cumulus clouds. *Journal of the Atmospheric Sciences*, 50(23), 3894–3908. [https://doi.org/10.1175/1520-0469\(1993\)050\(3894:LESOTW\)2.0.CO;2](https://doi.org/10.1175/1520-0469(1993)050(3894:LESOTW)2.0.CO;2)

Dai, Y., Dickinson, R. E., & Wang, Y.-P. (2004). A two-big-leaf model for canopy temperature, photosynthesis, and stomatal conductance. *Journal of Climate*, 17(12), 2281–2299. [https://doi.org/10.1175/1520-0442\(2004\)017<2281:atmfc>2.0.co;2](https://doi.org/10.1175/1520-0442(2004)017<2281:atmfc>2.0.co;2)

Denmead, O. T., & Bradley, E. F. (1985). Flux-gradient relationships in a forest canopy. In B. A. Hutchison & B. B. Hicks (Eds.), *The forest-atmosphere interaction: Proceedings of the forest environmental measurements conference held at Oak Ridge, Tennessee, October 23–28, 1983* (pp. 421–442). Springer Netherlands. https://doi.org/10.1007/978-94-009-5305-5_27

de Wit, C. (1965). Photosynthesis of leaf canopies (Technical Report). Retrieved from <https://edepot.wur.nl/187115>

Dias-Junior, C. Q., Dias, N. L., dos Santos, R. M. N., Sörgel, M., Araújo, A., Tsokankunku, A., et al. (2019). Is there a classical inertial sublayer over the Amazon forest? *Geophysical Research Letters*, 46(10), 5614–5622. <https://doi.org/10.1029/2019GL083237>

Durand, M., Murchie, E. H., Lindfors, A. V., Urban, O., Aphalo, P. J., & Robson, T. M. (2021). Diffuse solar radiation and canopy photosynthesis in a changing environment. *Agricultural and Forest Meteorology*, 311, 108684. <https://doi.org/10.1016/j.agrformet.2021.108684>

Dwyer, M. J., Patton, E. G., & Shaw, R. H. (1997). Turbulent kinetic energy budgets from a large-eddy simulation of airflow above and within a forest canopy. *Boundary-Layer Meteorology*, 84(1), 23–43. <https://doi.org/10.1023/A:1000301303543>

Fang, H. (2021). Canopy clumping index (CI): A review of methods, characteristics, and applications. *Agricultural and Forest Meteorology*, 303, 108374. <https://doi.org/10.1016/j.agrformet.2021.108374>

Farquhar, G. D., von Caemmerer, S., & Berry, J. A. (1980). A biochemical model of photosynthetic CO_2 assimilation in leaves of C_3 species. *Planta*, 149(1), 78–90. <https://doi.org/10.1007/BF00386231>

Finnigan, J. J., Shaw, R. H., & Patton, E. G. (2009). Turbulence structure above a vegetation canopy. *Journal of Fluid Mechanics*, 637, 387–424. <https://doi.org/10.1017/S0022112009990589>

Fu, Z., Gerken, T., Bromley, G., Araújo, A., Bonal, D., Burban, B., et al. (2018). The surface-atmosphere exchange of carbon dioxide in tropical rainforests: Sensitivity to environmental drivers and flux measurement methodology. *Agricultural and Forest Meteorology*, 263, 292–307. <https://doi.org/10.1016/j.agrformet.2018.09.001>

Fuentes, J. D., Chamecki, M., dos Santos, R. M. N., Randow, C. V., Stoy, P. C., Katul, G., et al. (2016). Linking meteorology, turbulence, and air chemistry in the Amazon rain forest. *Bulletin of the American Meteorological Society*, 97(12), 2329–2342. <https://doi.org/10.1175/BAMS-D-15-00152.1>

Gentine, P., Massmann, A., Lintner, B. R., Hamed Alemohammad, S., Fu, R., Green, J. K., et al. (2019). Land-atmosphere interactions in the tropics – A review. *Hydrology and Earth System Sciences*, 23(10), 4171–4197. <https://doi.org/10.5194/hess-23-4171-2019>

Goudriaan, J., & van Laar, H. (1994). *Modelling potential crop growth processes: Textbook with exercises* (Vol. 2). Kluwer Academic Publishers.

Griffis, T. J. (2013). Tracing the flow of carbon dioxide and water vapor between the biosphere and atmosphere: A review of optical isotope techniques and their application. *Agricultural and Forest Meteorology*, 174–175, 85–109. <https://doi.org/10.1016/j.agrformet.2013.02.009>

Helbig, M., Gerken, T., Beamesderfer, E. R., Baldocchi, D. D., Banerjee, T., Biraud, S. C., et al. (2021). Integrating continuous atmospheric boundary layer and tower-based flux measurements to advance understanding of land-atmosphere interactions. *Agricultural and Forest Meteorology*, 307, 108509. <https://doi.org/10.1016/j.agrformet.2021.108509>

Hernández, G. G., Winter, K., & Slot, M. (2020). Similar temperature dependence of photosynthetic parameters in sun and shade leaves of three tropical tree species. *Tree Physiology*, 40(5), 637–651. <https://doi.org/10.1093/treephys/paa015>

Heus, T., van Heerwaarden, C. C., Jonker, H. J. J., Pier Siebesma, A., Axelsen, S., van den Dries, K., et al. (2010). Formulation of the Dutch Atmospheric Large-Eddy Simulation (DALES) and overview of its applications. *Geoscientific Model Development*, 3(2), 415–444. <https://doi.org/10.5194/gmd-3-415-2010>

Iacono, M. J., Delamere, J. S., Mlawer, E. J., Shephard, M. W., Clough, S. A., & Collins, W. D. (2008). Radiative forcing by long-lived greenhouse gases: Calculations with the AER radiative transfer models. *Journal of Geophysical Research*, 113(D13), D13103. <https://doi.org/10.1029/2008JD009944>

Jacobs, C. M. J., & de Bruin, H. A. R. (1997). Predicting regional transpiration at elevated atmospheric CO_2 : Influence of the PBL-vegetation interaction. *Journal of Applied Meteorology*, 36(12), 1663–1675. [https://doi.org/10.1175/1520-0450\(1997\)036\(1663:PRTAEA\)2.0.CO;2](https://doi.org/10.1175/1520-0450(1997)036(1663:PRTAEA)2.0.CO;2)

Jacobs, C. M. J., van den Hurk, B., & de Bruin, H. (1996). Stomatal behaviour and photosynthetic rate of unstressed grapevines in semi-arid conditions. *Agricultural and Forest Meteorology*, 80(2), 111–134. [https://doi.org/10.1016/0168-1923\(95\)02295-3](https://doi.org/10.1016/0168-1923(95)02295-3)

Joseph, J. H., Wiscombe, W. J., & Weinman, J. A. (1976). The Delta-Eddington approximation for radiative flux transfer. *Journal of the Atmospheric Sciences*, 33(12), 2452–2459. [https://doi.org/10.1175/1520-0469\(1976\)033\(2452:TDEAFR\)2.0.CO;2](https://doi.org/10.1175/1520-0469(1976)033(2452:TDEAFR)2.0.CO;2)

Katul, G. G., Oren, R., Manzoni, S., Higgins, C., & Parlange, M. B. (2012). Evapotranspiration: A process driving mass transport and energy exchange in the soil-plant-atmosphere-climate system. *Reviews of Geophysics*, 50(3). <https://doi.org/10.1029/2011RG000366>

Kobayashi, H., Baldocchi, D. D., Ryu, Y., Chen, Q., Ma, S., Osuna, J. L., & Ustin, S. L. (2012). Modeling energy and carbon fluxes in a heterogeneous oak woodland: A three-dimensional approach. *Agricultural and Forest Meteorology*, 152, 83–100. <https://doi.org/10.1016/j.agrformet.2011.09.008>

LeMone, M. A., Angevine, W. M., Bretherton, C. S., Chen, F., Dudhia, J., Fedorovich, E., et al. (2019). 100 years of progress in boundary layer meteorology. *Meteorological Monographs*, 59, 9.1–9.85. <https://doi.org/10.1175/AMSMONOGRAPH-D-18-0013.1>

Leuning, R., Kelliher, F. M., de Pury, D. G. G., & Schultz, E.-D. (1995). Leaf nitrogen, photosynthesis, conductance and transpiration: Scaling from leaves to canopies. *Plant, Cell & Environment*, 18(10), 1183–1200. <https://doi.org/10.1111/j.1365-3040.1995.tb00628.x>

Ma, Y., & Liu, H. (2019). An advanced multiple-layer canopy model in the WRF model with large-eddy simulations to simulate canopy flows and scalar transport under different stability conditions. *Journal of Advances in Modeling Earth Systems*, 11(7), 2330–2351. <https://doi.org/10.1029/2018MS001347>

Machado, L. A. T., Dias, M. A. F. S., Morales, C., Fisch, G., Vila, D., Albrecht, R., et al. (2014). The CHUVA project: How does convection vary across Brazil? *Bulletin of the American Meteorological Society*, 95(9), 1365–1380. <https://doi.org/10.1175/BAMS-D-13-00084.1>

Martin, S. T., Artaxo, P., Machado, L. A. T., Manzi, A. O., Souza, R. A. F., Schumacher, C., et al. (2016). Introduction: Observations and modeling of the Green Ocean Amazon (GoAmazon2014/5). *Atmospheric Chemistry and Physics*, 16(8), 4785–4797. <https://doi.org/10.5194/acp-16-4785-2016>

Massmann, A., Gentile, P., & Lin, C. (2019). When does vapor pressure deficit drive or reduce evapotranspiration? *Journal of Advances in Modeling Earth Systems*, 11(10), 3305–3320. <https://doi.org/10.1029/2019MS001790>

Maurer, K. D., Bohrer, G., Kenny, W. T., & Ivanov, V. Y. (2015). Large-eddy simulations of surface roughness parameter sensitivity to canopy-structure characteristics. *Biogeosciences*, 12(8), 2533–2548. <https://doi.org/10.5194/bg-12-2533-2015>

Monteith, J. (1965). Evaporation and environment. *Symposia of the Society for Experimental Biology*, 19, 205–234.

Moon, Z., Fuentes, J. D., & Staebler, R. M. (2020). Impacts of spectrally resolved irradiance on photolysis frequency calculations within a forest canopy. *Agricultural and Forest Meteorology*, 291, 108012. <https://doi.org/10.1016/j.agrformet.2020.108012>

Nieuwstadt, F. T. M., & Brost, R. A. (1986). The decay of convective turbulence. *Journal of the Atmospheric Sciences*, 43(6), 532–546. [https://doi.org/10.1175/1520-0469\(1986\)043\(0532:TDOCT\)2.0.CO;2](https://doi.org/10.1175/1520-0469(1986)043(0532:TDOCT)2.0.CO;2)

Nikolov, N. T., Massman, W. J., & Schoettle, A. W. (1995). Coupling biochemical and biophysical processes at the leaf level: An equilibrium photosynthesis model for leaves of C_3 plants. *Ecological Modelling*, 80(2), 205–235. [https://doi.org/10.1016/0304-3800\(94\)00072-P](https://doi.org/10.1016/0304-3800(94)00072-P)

Nilson, T. (1971). A theoretical analysis of the frequency of gaps in plant stands. *Agricultural Meteorology*, 8, 25–38. [https://doi.org/10.1016/0002-1571\(71\)90092-6](https://doi.org/10.1016/0002-1571(71)90092-6)

Norman, J. (1979). Modeling the complete crop canopy. In B. J. Barfield & J. F. Gerber (Eds.), *Modification of the Aerial Environment of Crops* (pp. 249–280).

Ouwersloot, H. G., Moene, A. F., Attema, J. J., & de Arellano, J. V.-G. (2016). Large-eddy simulation comparison of neutral flow over a canopy: Sensitivities to physical and numerical conditions, and similarity to other representations. *Boundary-Layer Meteorology*, 162, 1–19. <https://doi.org/10.1007/s10546-016-0182-5>

Patton, E. G., Horst, T. W., Sullivan, P. P., Lenschow, D. H., Oncley, S. P., Brown, W. O. J., et al. (2011). The canopy horizontal array turbulence study. *Bulletin of the American Meteorological Society*, 92(5), 593–611. <https://doi.org/10.1175/2010BAMS2614.1>

Patton, E. G., Sullivan, P., & Davis, K. (2003). The influence of a forest canopy on top-down and bottom-up diffusion in the planetary boundary layer. *Quarterly Journal of the Royal Meteorological Society*, 129(590), 1415–1434. <https://doi.org/10.1256/qj.01.175>

Patton, E. G., Sullivan, P. P., Shaw, R. H., Finnigan, J. J., & Weil, J. C. (2016). Atmospheric stability influences on coupled boundary layer and canopy turbulence. *Journal of the Atmospheric Sciences*, 73(4), 1621–1647. <https://doi.org/10.1175/JAS-D-15-0068.1>

Pedruzo-Bagazgoitia, X. (2022a). Dales4.2_canopy [Dataset]. Zenodo. <https://doi.org/10.5281/zenodo.6582455>

Pedruzo-Bagazgoitia, X. (2022b). Scripts and observations for Pedruzo-Bagazgoitia et al. (2022) [Dataset]. Zenodo. <https://doi.org/10.5281/zenodo.6582524>

Pedruzo-Bagazgoitia, X., Ouwersloot, H. G., Sikma, M., van Heerwaarden, C. C., Jacobs, C. M. J., & Vilà-Guerau de Arellano, J. (2017). Direct and diffuse radiation in the shallow cumulus–vegetation system: Enhanced and decreased evapotranspiration regimes. *Journal of Hydrometeorology*, 18(6), 1731–1748. <https://doi.org/10.1175/JHM-D-16-0279.1>

Powers, J. G., Klemp, J. B., Skamarock, W. C., Davis, C. A., Dudhia, J., Gill, D. O., et al. (2017). The weather research and forecasting model: Overview, system efforts, and future directions. *Bulletin of the American Meteorological Society*, 98(8), 1717–1737. <https://doi.org/10.1175/BAMS-D-15-00308.1>

Ronda, R. J., de Bruin, H. A. R., & Holtslag, A. A. M. (2001). Representation of the canopy conductance in modeling the surface energy budget for low vegetation. *Journal of Applied Meteorology*, 40(8), 1431–1444. [https://doi.org/10.1175/1520-0450\(2001\)040\(1431:ROTCCI\)2.0.CO;2](https://doi.org/10.1175/1520-0450(2001)040(1431:ROTCCI)2.0.CO;2)

Shaw, R. H., & Patton, E. G. (2003). Canopy element influences on resolved- and subgrid-scale energy within a large-eddy simulation. *Agricultural and Forest Meteorology*, 115(1), 5–17. [https://doi.org/10.1016/S0168-1923\(02\)00165-X](https://doi.org/10.1016/S0168-1923(02)00165-X)

Shaw, R. H., & Schumann, U. (1992). Large-eddy simulation of turbulent flow above and within a forest. *Boundary-Layer Meteorology*, 61(1), 47–64. <https://doi.org/10.1007/BF02033994>

Shettle, E. P., & Weinman, J. A. (1970). The transfer of solar irradiance through inhomogeneous turbid atmospheres evaluated by Eddington's approximation. *Journal of the Atmospheric Sciences*, 27(7), 1048–1055. [https://doi.org/10.1175/1520-0469\(1970\)027\(1048:TTOSIT\)2.0.CO;2](https://doi.org/10.1175/1520-0469(1970)027(1048:TTOSIT)2.0.CO;2)

Sikma, M., Ouwersloot, H. G., Pedruzo-Bagazgoitia, X., van Heerwaarden, C. C., & Vilà-Guerau de Arellano, J. (2018). Interactions between vegetation, atmospheric turbulence and clouds under a wide range of background wind conditions. *Agricultural and Forest Meteorology*, 255, 31–43. <https://doi.org/10.1016/j.agrformet.2017.07.001>

Sikma, M., Vilà-Guerau de Arellano, J., Pedruzo-Bagazgoitia, X., Voskamp, T., Heusinkveld, B., Anten, N., & Evers, J. (2019). Impact of future warming and enhanced $[CO_2]$ on the vegetation-cloud interaction. *Journal of Geophysical Research: Atmospheres*, 124(23), 12444–12454. <https://doi.org/10.1029/2019JD030717>

van der Laan-Luijkx, I. T., van der Velde, I. R., Krol, M. C., Gatti, L. V., Domingues, L. G., Correia, C. S. C., et al. (2015). Response of the Amazon carbon balance to the 2010 drought derived with CarbonTracker South America. *Global Biogeochemical Cycles*, 29(7), 1092–1108. <https://doi.org/10.1002/2014GB005082>

van Diepen, K. H. H., Goudriaan, J., Vilà-Guerau de Arellano, J., & de Boer, H. J. (2022). Comparison of C_3 photosynthetic responses to light and CO_2 predicted by the leaf photosynthesis models of Farquhar et al. (1980) and Goudriaan et al. (1985). *Journal of Advances in Modeling Earth Systems*, 14(9), e2021MS002976. <https://doi.org/10.1029/2021MS002976>

Vilà-Guerau de Arellano, J., Koren, G., Ouwersloot, H. G., van der Velde, I., Röckmann, T., & Miller, J. B. (2019). Sub-diurnal variability of the carbon dioxide and water vapor isotopologues at the field observational scale. *Agricultural and Forest Meteorology*, 275, 114–135. <https://doi.org/10.1016/j.agrformet.2019.05.014>

Vilà-Guerau de Arellano, J., Ney, P., Hartogensis, O., de Boer, H., van Diepen, K., Emin, D., et al. (2020). Cloudroots: Integration of advanced instrumental techniques and process modelling of sub-hourly and sub-kilometre land–atmosphere interactions. *Biogeosciences*, 17(17), 4375–4404. <https://doi.org/10.5194/bg-17-4375-2020>

Vilà-Guerau de Arellano, J., Ouwersloot, H. G., Baldocchi, D., & Jacobs, C. M. J. (2014). Shallow cumulus rooted in photosynthesis. *Geophysical Research Letters*, 41(5), 1796–1802. <https://doi.org/10.1002/2014GL059279>

Vilà-Guerau de Arellano, J., van Heerwaarden, C. C., van Stratum, B. J., & van den Dries, K. (2015). *Atmospheric boundary layer: Integrating air chemistry and land interactions*. Cambridge University Press. <https://doi.org/10.1017/CBO9781316117422>

Vilà-Guerau de Arellano, J., Wang, X., Pedruzo-Bagazgoitia, X., Sikma, M., Agusti-Panareda, A., Bousetta, S., et al. (2020). Interactions between the Amazonian rainforest and cumuli clouds: A large-eddy simulation, high-resolution ECMWF, and observational intercomparison study. *Journal of Advances in Modeling Earth Systems*, 12(7), e2019MS001828. <https://doi.org/10.1029/2019MS001828>

Williams, K., Gornall, J., Harper, A., Wilshire, A., Hemming, D., Quaife, T., et al. (2017). Evaluation of JULES-crop performance against site observations of irrigated maize from Mead, Nebraska. *Geoscientific Model Development*, 10(3), 1291–1320. <https://doi.org/10.5194/gmd-10-1291-2017>